Centennial-scale Oscillations of the Atlantic Meridional Overturning Circulation in Freshwater Experiments with the Bern3D Model

Master's Thesis

Faculty of Science
University of Bern

presented by
Eveline Lehmann
2011

Supervisor:
Prof. Dr. T. Stocker
Co-Supervisor:
PD Dr. Ch. Raible

Department for Climate and Environmental Physics
Physics Institute, University of Bern

Contents

Chapter 1

Introduction and Overview

Climate modeling is an important aspect of climate research. It allows a better and more quantitative understanding of relevant mechanisms of climate change and provides a tool for future climate projections. Although climate models are a simplification of the real world and contain many parametrizations of processes, they are based on the knowledge about basic chemical and physical mechanisms in the earth system. They are used as a quantitative approach to test scientific hypotheses of past and future climate change and help with the interpretation of paleoclimatic proxy data from ice cores, marine sediment cores, tree-rings and other archives.

It is not possible to include all known key processes which operate in the climate system in one single model, since this would exceed the computational power and storage capacity of any computer. Because of this, a large number of climate models exists which differ in their complexity and their representation of climate processes. The qualities of a climate model determine the field of application. Simplified models of zero or one dimension allow to assess a single, global-scale climate process, while three-dimensional coupled climate models represent the ocean and the atmosphere. These latter models compute the exchange of heat, moisture and momentum between the ocean and the atmosphere and are often also coupled to an ice-sheet model or a biosphere model, however, these complex models are very costly to run due to their high spatial and temporal resolution.

For the present thesis, the Bern3D model was used. It is a three-dimensional, cost efficient climate model of reduced complexity. Due to the coarse temporal and spatial resolution it is possible to perform a large number of simulations. In summer 2009, the model was coupled to an energy and moisture balance model (EBM). For this purpose, the world mask was modified and the Indonesian Passage and the Bering Strait were opened for barotropic flow. Model simulations with this new ocean bathymetry have so far only been tuned for experiments coupled with the EBM. However, no model simulations with the open passages have been performed using only the ocean part of the model under mixed-boundary conditions.

A number of freshwater perturbation experiments were performed in order to analyze the response of the Atlantic meridional overturning circulation (MOC) to freshwater pulses into the ocean when applying the modified bathymetry. In some model experiments, oscillations were found in the Atlantic MOC which have not been seen before the opening of the two passages. Oscillations in model simulations could be an indicator for numerical instabilities

of the model. However, they can also be linked to a negative physical feedback mechanism within the climate system, which prevents the system to acquire another stable state.

The focus of this thesis is to investigate the impact of freshwater forcing experiments on the Atlantic MOC using the modified world mask and variants, and to understand the appearance of oscillations in the overturning circulation in terms of their physical and numerical background.

Chapter 2 gives an introduction to the large-scale ocean circulation and shows the importance of deep water formation in the North Atlantic on the stability of the MOC.

The ocean part of the Bern3D model is briefly introduced in chapter 3. Also, the new world with the open Bering Strait and Indonesian Passage is described and additionally, three newly created world settings are introduced. Their purpose is to investigate the origin of the oscillations.

In chapter 4, the model spinup process is described, and the different steady states of the four world masks used in this thesis are compared.

A number of freshwater perturbation experiments are shown in chapter 5 and the different states of the MOC after freshwater perturbations are analyzed.

Chapter 6 investigates the oscillations in the Atlantic MOC during freshwater perturbation experiments. A sensitivity study with the four different world masks is performed and the characteristics of the oscillations are discussed. A physical feedback mechanism and numerical instabilities in the model are presented as a possible cause for the oscillations.

Finally, a summary of the results of this thesis and an outlook to future work with the Bern3D model is provided in chapter 7.

Chapter 2

Large-Scale Ocean Circulation

2.1 The Meridional Overturning Circulation

About 70% of the Earth's surface is covered by ocean. With the ability to store an immense amount of heat and to redistribute this energy, the ocean plays an important role in the Earth's climate system. In low latitudes, the radiative balance at the top of the atmosphere is positive, leading to a surplus of energy, while the high latitudes and the polar regions experience a net loss of radiative energy. This imbalance of the energy budget is compensated by a meridional heat transport from the tropics towards the poles; about half of this energy is transported by the ocean circulation [*Stocker*, 2000]. The globally integrated meridional heat flux is shown in Fig. 2.1(left). More heat is lost in the Northern Hemisphere than in the Southern Hemisphere. Meridional heat transport towards the north can be observed in the Atlantic and in the Pacific (Fig. 2.1(right)), however, due to the configuration of the ocean basins, only the Atlantic Ocean can transport heat all the way to the polar region.

The regional pattern of the ocean basins, action of wind, and atmosphere-ocean heat and freshwater fluxes result in a number of ocean currents which transport momentum and energy, in both the horizontal and the vertical direction. The large-scale surface circulation is driven

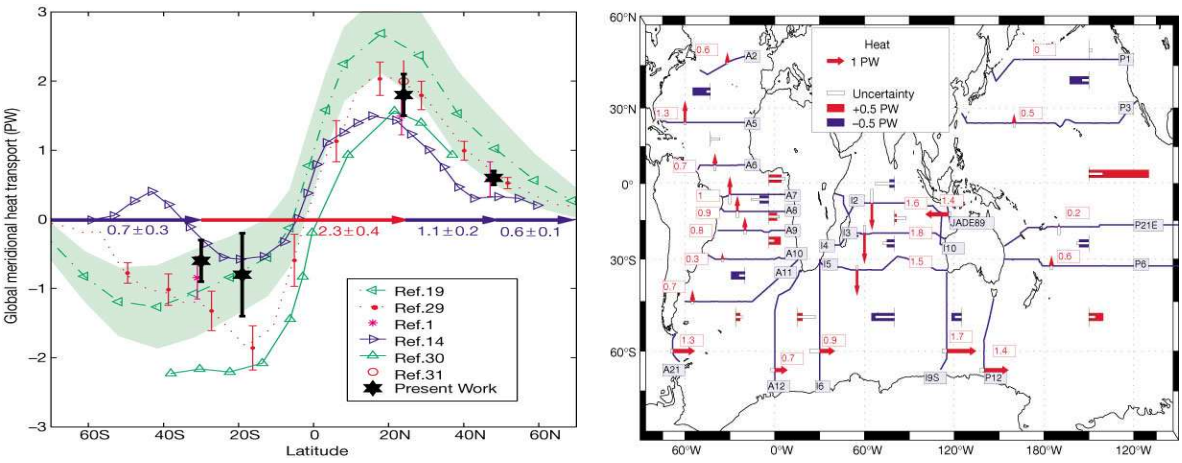

Figure 2.1: Global averaged meridional heat transport (left) and transoceanic heat transport (left) based on the study of *Ganachaud and Wunsch* [2000].

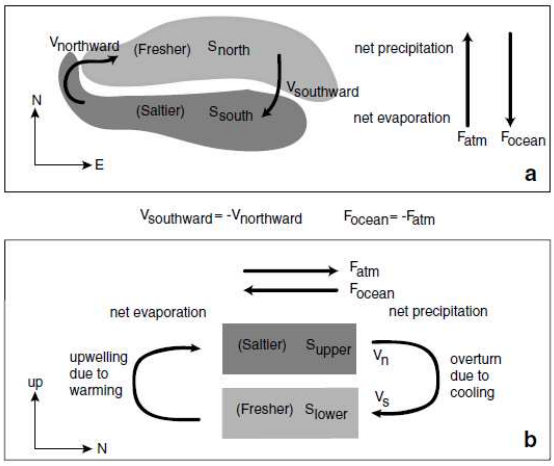

Figure 2.2: Schematical illustration of the transport of ocean water a) in the horizontal direction between the low and the high latitudes and b) in the vertical direction associated with the gain of density due to the cooling of saline water in the North Atlantic [*Talley*, 2008].

primarily by wind stress whereas the deep ocean circulation is mostly driven by differences is the density of ocean water linked to positive salinity and temperature anomalies. In the tropical regions of the Atlantic Ocean, water takes up heat from the solar irradiation and evaporates, which increases the sea surface salinity (SSS). When the water flows northwards, it cools by loosing heat to the atmosphere. At the same time it increases its density, since sea water with a low temperature and high salinity has a higher density [*Pond and Pickard*, 1983]. A schematic illustration of this process is shown in Fig. 2.2. The water sinks in the Greenland-Iceland-Norwegian (GIN) Sea and in the Labrador Sea, forming North Atlantic Deep Water (NADW), which is transported southward and is either exported into the Southern Ocean or recirculates in the Atlantic Ocean [*Talley*, 2008]. A similar process takes place in the Southern Ocean, namely in the Ross and the Weddell Seas, where Antarctic Bottom Water (AABW) is formed. The sinking of the water is compensated by an upwelling in the Pacific and the Indian Oceans. The concept of an inter-basin exchange of water masses was first proposed by *Stommel* [1958] and then termed *Conveyor Belt* by *Broecker* [1987]. Today, it is called Meridional Overturning Circulation (MOC). Since the physical drivers for this large-scale circulation are temperature and salinity gradients, it is also known as the Thermohaline Circulation (THC). A simplified illustration of the THC is presented in Fig. 2.3.

2.2 Freshwater in the North Atlantic Ocean

The last ice age, lasting from about 110 - 12 kyr before present (BP, i.e., before 1950), was characterized by a series of abrupt climate changes, usually linked with a decrease of the MOC. Dansgaard-Oeschger (D-O) events are periods in time during the pas 120 kyr with are linked to very pronounced climate change. They are characterized by a rapid warming within a few decades, followed by slow cooling, which lasted a few centuries [*Rahmstorf*, 2002; *Stocker*, 2000; and references therein]. Based on ice core records of Greenland, 17 of this D-O events were dated, their duration was about 1,000 - 3,000 years. The impact of these events was most pronounced in the Northern Hemisphere, however, also ice core records

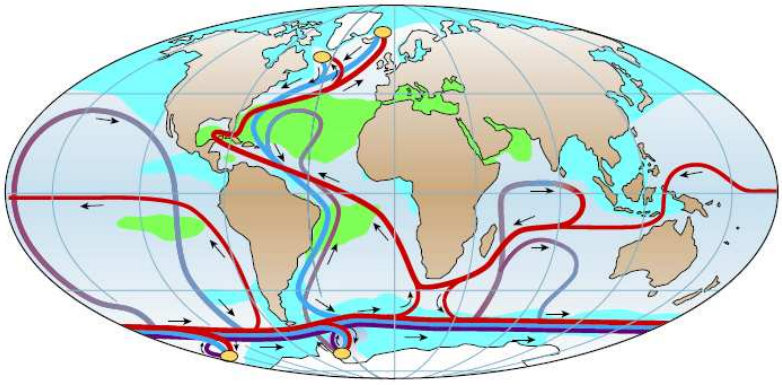

Figure 2.3: Simplified illustration of the global ocean circulation. Near-surface waters (red lines) flow towards the main deep water formation regions in the North Atlantic and near Antarctica (yellow points) where the water sinks and recirculates in depth (blue indicates the deep currents and purple the bottom currents). Green shaded areas have SSS higher than 36‰, values below 34‰ are shaded blue [*Rahmstorf*, 2002].

from Antarctica reveal climate variabilities during D-O events, suggesting an interhemispheric connection [*Stocker and Johnsen*, 2003; *Barker et al.*, 2009].

In ocean sediment cores from the North Atlantic, *Heinrich* [1988] documented layers of coarse fragments. The particles are so called ice-rafted debris, thus sediment which was transported in glaciers and underneath floating ice bergs, and has been deposited to the ocean ground when the ice has melted. The layers were found within six time intervals during the last glaciation and they were labeled H1 to H6, where H1 is the youngest of the six events [*Hemming*, 2004; and references therein]. It is believed that the ice originated from the eastern portion of the Laurentide ice sheet, which was drained into the Hudson Strait [*Hemming*, 2004]. The Heinrich layers are evidence for rapid expansions in the ice sheets of the Northern Hemisphere. *Bond et al.* [1999] suggested a link to climate shifts which must have caused these enormous ice surges and collapses of parts of the ice sheet into the Hudson Strait. However, the formation of Heinrich layers is still poorly understood, but it is known that they occurred during extreme cold periods in the North Atlantic and were followed by a dramatic warming, the D-O events, well known from Greenland ice cores [*Hemming*, 2004; *NGRIP*, 2004]. The Heinrich events were coupled to an inflow of large amounts of freshwater into the North Atlantic, and it appears that they were associated with a shutdown of the formation of NADW [*Hemming*, 2004].

The Younger Dryas (YD) was the last of these abrupt cooling events before the beginning of the Holocene warm epoch. It is dated in the period from 12,800 - 11,500 BP. It is assumed that the warming which preceded the YD, the Bølling-Allerød period, caused the initiation of retreat of the Laurentide ice sheet and the accumulation of large amounts of melt water in the Lake Agassiz. This lead to a large discharge of freshwater in the Hudson Bay and with this to a significant slowdown of the Atlantic MOC and a cooling in the Northern Hemisphere [*Broecker et al.*, 1988; *Rahmstorf*, 2002; *McManus et al.*, 2004].

Freshwater perturbation experiments in model simulations help to better understand and quantify such rapid climate changes of the past and to make predictions of future changes in

the large-scale ocean circulation.

Chapter 3

The Bern3D Ocean Model

The Bern3D model is a global three-dimensional earth-system model of intermediate complexity (EMIC), that consists of a two-dimensional energy balance model that is coupled to a three-dimensional ocean model. The model has a coarse resolution and was developed to perform long-term simulations on glacial-to-interglacial timescales. With the capacity to calculate 50,000 model years per day on one single personal-computer CPU, the Bern3D climate model is very cost efficient [*Ritz et al.*, 2011]. Such a climate model has the ability to test the sensitivity of a large number of parameters on a global scale and allows a basic understanding of long-term climate variability. The three-dimensional ocean has the benefit to directly represent the fundamental frictional-geostrophic momentum balance. Therefore, horizontal gyre circulations, the effects of ocean topography and changes in the location of deep water formation can be represented, allowing a basic understanding of the ocean circulation [*Edwards and Marsh*, 2005].

For this thesis, only the ocean part of the Bern3D model was used. An overview on the physics of this model component and the elements used for the thesis is given in this chapter.

3.1 General description of the model

The Bern3D ocean model is based on the model of *Edwards et al.* [1998] and *Edwards and Marsh* [2005] and described in detail by *Müller et al.* [2006].

The model has a coarse temporal and spatial resolution, resulting in a high computational efficiency. 48 time steps are calculated per year, which makes about one time step per week. The ocean is resolved by 36 $\times$ 36 grid boxes in the horizontal direction and 32 layers in depth. The horizontal grid boxes are equidistant in longitude and in the sine of latitude. This makes the boxes of equal surface area. On the vertical scale, the height of the layers decreases logarithmically with depth, where the uppermost layer has a thickness of only 38 meters while the box at the bottom achieves 397 meters. The maximum depth of the ocean is 5000 meters. The ocean has a fixed surface, thus no elevation change of the ocean surface can be considered. The volume of the ocean is constant at all times.

Scalar concentrations of tracers (e.g., temperature and salinity) are defined in the center of the boxes, while the box boundaries contain information on the velocity and diffusion components $\vec{u} = (u, v, w)$. The streamfunction Ψ is defined at the corners of the grid boxes.

The model has a seasonal forcing of temperature and salinity at the surface of the ocean and a seasonal wind stress forcing. Monthly data for sea surface temperature and salinity are derived from *Levitus et al.* [1994] and *Levitus and Boyer* [1994], monthly values for wind stress are taken from NCEP reanalysis data by *Kalnay et al.* [1996]. In order to enhance the strength of the wind-driven gyres, the wind stress values are scaled by a factor of two [*Edwards and Marsh*, 2005].

3.2 Governing Equations

The model is based on the frictional-geostrophic balance equations which represent the horizontal flow velocities u and v in the longitudinal and latitudinal direction (equation 3.1 and 3.2). The hydrostatic balance (equation 3.3) represents the pressure gradient in the z-direction. The equations are expressed in orthogonal spherical polar coordinates where ϕ is the longitude, θ is the latitude, and z the negative depth with a surface value of $z = 0$:

$$-fv = -\frac{1}{\rho r \cos\theta}\frac{\partial p}{\partial \phi} - \lambda u + \alpha\frac{\partial \tau_\phi}{\partial z}, \tag{3.1}$$

$$fu = -\frac{cos\theta}{\rho r}\frac{\partial p}{\partial (sin\theta)} - \lambda v + \alpha\frac{\partial \tau_{(\sin\theta)}}{\partial z}, \tag{3.2}$$

$$\frac{\partial p}{\partial t} = -g\rho(T, S), \tag{3.3}$$

where λ is a drag coefficient, τ the wind stress, $\alpha = 2$ a scaling factor for the wind stress, r the radius of the earth, g the gravitational acceleration and f the Coriolis parameter which is defined as

$$f = 2\Omega \sin\theta. \tag{3.4}$$

The local density is represented by ρ and depends only on temperature T and salinity S but not on the pressure [*Winton and Sarachik*, 1993]. The drag coefficient λ is increased near continental boundaries, shallow ocean topography and along the equator in order to avoid numerical instability [*Edwards and Marsh*, 2005].

The vertical velocity w is derived using the continuity equation with the assumption

$$\vec{\nabla} \cdot (\vec{u}) = 0. \tag{3.5}$$

Transport of tracers in the ocean is based on advection, diffusion, convection and sources minus sinks:

$$\frac{D}{Dt}X = \vec{\nabla} \cdot (\mathbf{A}\vec{\nabla}X) + \mathbf{C}X + \mathrm{SMS}, \tag{3.6}$$

where

$$\frac{D}{Dt}X = \frac{\partial}{\partial t} + \vec{u} \cdot (\vec{\nabla}X) \tag{3.7}$$

represents the material derivative of the tracer X in dependence of the diffusion matrix $\mathbf{A}$, the convective adjustment operator $\mathbf{C}$ and SMS, which stands for external sources minus sinks, e.g., net air-sea fluxes or the decay of radioactive tracers.

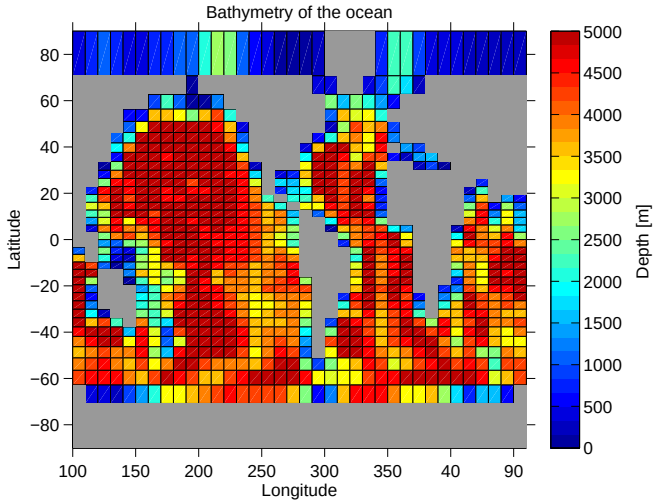

Figure 3.1: The bathymetry of the ocean (depth in m) in the Bern3D model.

3.3 Bathymetry of the ocean floor

The bathymetry of the ocean floor was derived by interpolation and Fourier filtering of realistic topography data (taken from ETOPO5, *NOAA* [1988]). With this, the ocean topography of the real world was approximated (Fig. 3.1). To increase the performance of the dynamics of the ocean, some adjustments to the topography have been made. The Drake Passage was widened and deepened to strengthen the Antarctic Circumpolar Current (ACC). The depth of the Greenland-Iceland-Norway (GIN) sea was increased to 824 meters in order to increase North Atlantic Deep Water (NADW) formation. Additionally, the ocean floor has been smoothed and filled in some parts of the ocean where no dynamics take place.

3.4 Restoring and mixed boundary conditions

Restoring boundary conditions (RBC) are used to calculate a first equilibrium state in the model where surface values of temperature and salinity are directly restored to measured data. This implies that the surface flux from the atmosphere to the ocean, F_{OA}, is a boundary condition and temperature and salinity are calculated using the following equations:

$$F_{OA}(T) = \frac{\Delta z}{\tau}(T - T^*), \tag{3.8}$$

$$F_{OA}(S) = \frac{\Delta z}{\tau}(S - S^*). \tag{3.9}$$

T^* and S^* are the observed values for temperature and salinity, derived from *Levitus et al.* [1994] and *Levitus and Boyer* [1994]. τ represents the relaxation time scale for the mixed layer depth Δz which in our model is the surface box with a depth of 39 m; τ is set to 19.5 days.

While RBC are a good approximation of the model to real data, a permanently restored flux of salinity in the model makes not much sense, since the adjustment of salinity and temperature distribution as a response to different climate conditions is governed by different processes in the climate system. Warming of the surface ocean, for example, leads to an increased evaporation (and precipitation), while a positive anomaly in sea surface salinity (SSS) does not necessary lead to precipitation. To uncouple the salinity flux (which in our case has a negative sign and therefore is the flux of moisture from the ocean to the atmosphere) the model is usually run under mixed boundary conditions (MBC):

$$F_{OA}(T) = \frac{\Delta z}{\tau}(T - T^*), \tag{3.10}$$

$$F_{OA}(S) = Q_s^*(t), \tag{3.11}$$

where a seasonal salt flux $Q_s^*(t)$ is diagnosed under RBC and then used for further simulations. With this notation, the density structure at the ocean surface is not fixed to prescribed observations but can vary with changing conditions. For instance, this makes changes in the global ocean circulation due to freshwater perturbations possible.

3.5 Convection and deep water formation

In case of instability in the ocean layers due to high-density water above water with lower density, convection in the water masses occurs. The transport flux that is necessary to keep the density field stable is represented by the convective adjustment operator $\mathbf{C}$ in equation (3.6). In the Bern3D ocean model two different convection schemes are applied. The "mixing" convection presented in the model version of *Edwards et al.* [1998] mixes and combines unstable levels with adjacent boxes to obtain a vertically uniform stratification at all times. In addition to this, a second convection scheme is used. The "shuffling" convection precedes the original convection algorithm with the purpose to remove instabilities of water density in the uppermost layer. The tracer properties of the surface box are inserted at the suitable depth just above the box with water denser than the water of the surface box. The boxes

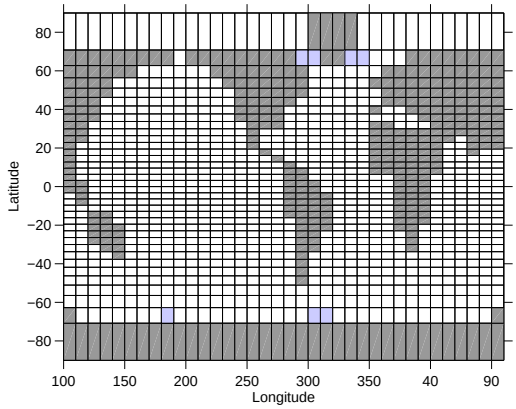

Figure 3.2: The four regions of deep water formation in the Bern3D model are shown in blue.

above are shifted upward by the vertical extent of the topmost layer. Since the height of the boxes decreases with depth, this shift leads to a mixing of the properties of each layer into the overlaying layer. Note that the shuffling convection is only used for the tracers temperature and salinity, but not for any other tracers. Once this "shuffling" convection is finished, the "mixing" convection removes remaining instabilities in the interior of the water column [*Müller et al.*, 2006].

The formation of deep water is strongly linked to the convection described above. Chapter 2.1 explained the physical background of the formation of North Atlantic Deep Water (NADW) and Antarctic Bottom Water (AABW). But since the Bern3D model has a very coarse resolution and no sea-ice formation is possible when running the model under MBC (Section 3.4), deep water formation in the model is limited due to insufficient convection. To increase the overturning circulation in the model, the salinity field of *Levitus et al.* [1994] used in equation (3.9) has been modified to higher values in some boxes of four regions, namely the GIN and the Labrador Seas in the North Atlantic and the Ross and Weddell Seas in the Southern Ocean (Fig. 3.2). This modification results in stronger deep water formation in these regions and therefore in a more realistic overturning circulation.

3.6 The different world masks

With the coupling of the energy balance model (EBM) to the Bern3D ocean model [*Ritz et al.*, 2011], a new world mask containing information on topography, islands and barotropic fluxes around the islands was developed. In addition to this, some adjustments in the world mask were done for the analysis described in this thesis.

This section describes the different world masks in detail, an overview can be found in Tab. 3.1 and Fig. 3.3.

The original world setup

The original world setup was the basis for a number of ocean model simulations under mixed boundary conditions [*Gerber and Joos*, 2010; *Gerber et al.*, 2009; *Ritz et al.*, 2008; *Parekh et al.*, 2008; *Tschumi et al.*, 2008; *Müller et al.*, 2008; *Siddall et al.*, 2007; *Muscheler et al.*, 2007]. Henceforth, the original setup is called "old world".

Name of setting	IP	BS	Depth of GS
"old world"	closed	diffusive flux only	1 box
"new world"	barotropic flux	barotropic flux	5 boxes
"world BS closed"	barotropic flux	closed	5 boxes
"world IP closed"	closed	barotropic flux	5 boxes
"world all closed"	closed	closed	5 boxes

Table 3.1: Overview of different world settings and the names used in this thesis. IP denotes the Indonesian Passage, BS the Bering Strait, and GS the Gibraltar Strait.

The ocean topography of the "old world" is the same as described in section 3.3. The Bering Strait (BS) and the Gibraltar Strait (GS) have a depth of only one single box (39 m). These passages remain closed for the barotropic flow. Only diffusive transport is possible between the Pacific and the Arctic Ocean and the Mediterranean Sea and the Atlantic, respectively. Also the Indonesian Passage (IP) remains completely closed where the Australian continent is linked to Indonesia. Antarctica is the only island surrounded by a closed barotropic flux. The rest of the continents build one large island with no flows through straits.

The new world setup

The new setup was developed in summer 2009 to run the ocean model coupled to the EBM. It is the new standard setup used for recent and upcoming simulations with the Bern3D model [*Ritz et al.*, 2011]. Fig. 3.3a shows the surface of this standard setup, which is called "new world" in this thesis. The main new feature is the opening of the BS and the IP to permit barotropic flow. This implies that Australia and America are now also defined as islands. Together with Antarctica, there are now three islands in the model. The dynamical, barotropic flow around islands, and therefore through straits, is derived by the integration of the depth-averaged momentum equation (equations 3.1 and 3.2) around each island [*Edwards and Marsh*, 2005]. A further adjustment in the bathymetry is the deepening of the GS from one to five boxes (284 meters), which enhances the mixing of highly saline water from the Mediterranean Sea with the Atlantic.

Three modified world setups

In order to detect the effect of the two open passages (BS and IP) on the MOC, three additional world masks were created. Note that these additional world masks serve to investigate sensitivities in this thesis but will not be used for further model simulations. All three world setups are based on the "new world" where the opened passages BS and IP are alternately closed, i.e., linked to the continent. In this thesis, the world in which the BS is closed is called "world BS closed", the world with the closed IP is called "world IP closed" and the setup where both passages are closed is called "world all closed" in this thesis. Tab. 3.1 gives an overview on the different names and Fig. 3.3b-d shows the changes of the three modified world masks in relation to the "new world" (Fig. 3.3a).

In the prescribed world mask, the ocean has a maximum depth of 32 boxes, while the land masses is parametrized with values larger than 90. To close the straits in the modified setups, the value of the ocean is replaced by 91 in the file containing information on bathymetry. Further, the number of islands has been altered from three to two ("world BS closed" and "world IP closed") and one ("world all closed"), respectively. In addition to this, the integral of the barotropic streamfunction [*Edwards and Marsh*, 2005] around Australia (for "world IP closed") and America (for "world BS closed") was removed in order to link the islands to the continent.

3.7 Atlantic-to-Pacific freshwater flux

Salinity distribution in the North Atlantic plays an important role in stabilizing the Atlantic MOC as described in Chapter 2.1. In contrast to the Pacific, the North Atlantic is about

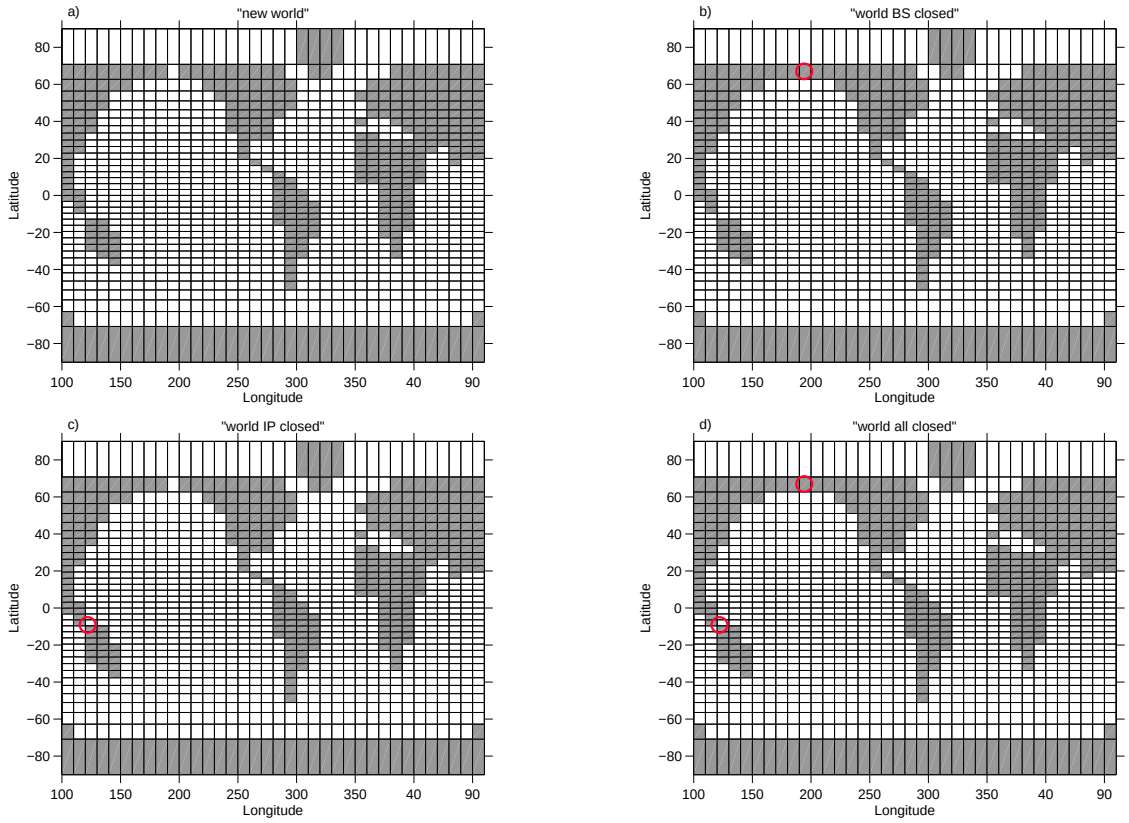

Figure 3.3: The four different world settings used in this study. The changes with respect to the "new world"are indicated with red circles.

1 psu more salty which leads to the stronger sinking of dense water in high latitudes and therefore to an increased deep water formation. The difference in salinity is mainly due to the imbalance in the freshwater budget with a net evaporation in the Atlantic Ocean and a

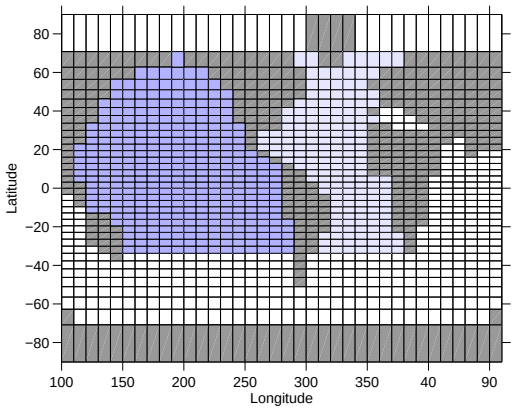

Figure 3.4: The region in the Atlantic (light blue) where the freshwater correction flux is subtracted and added in the Pacific (dark blue).

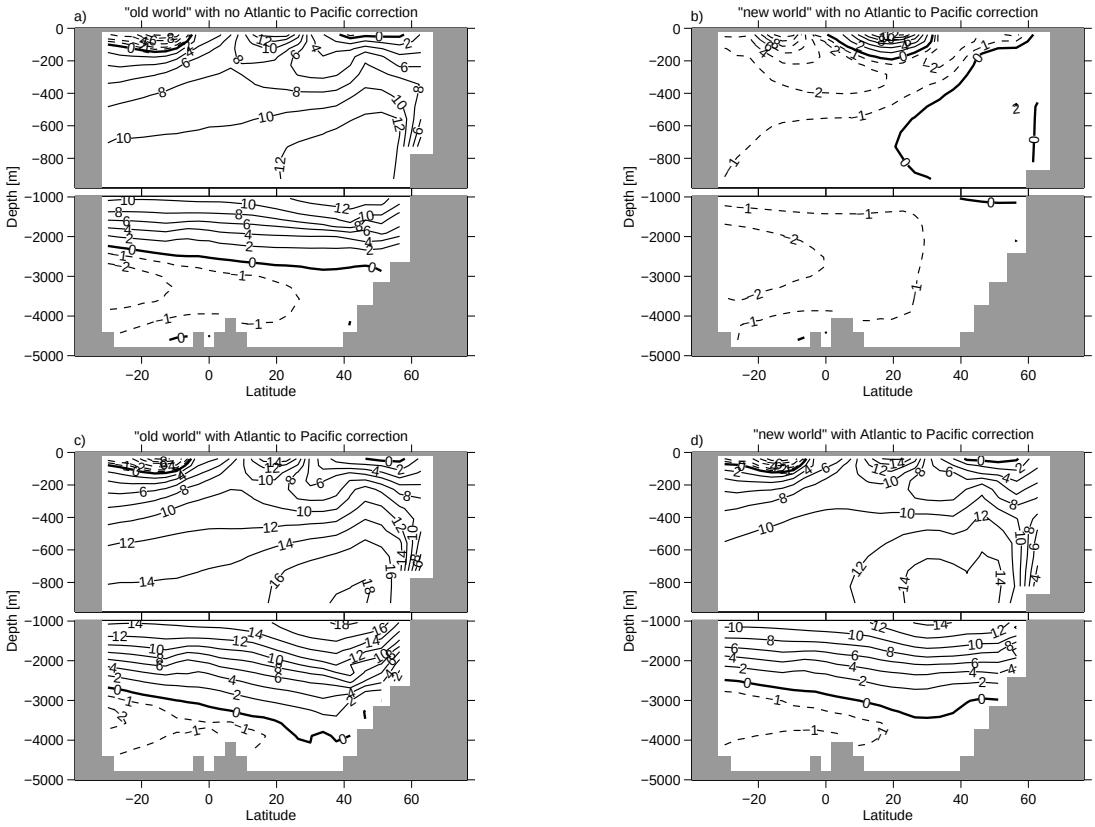

Figure 3.5: Streamfunction [Sv] of the maximum annual mean overturning circulation in the Atlantic for the "old world" (a and c) and the "new world" (band d).

net precipitation and runoff in the Pacific Ocean [*Talley*, 2008; *Zaucker et al.*, 1994]. This implies net vapor transport in the atmosphere from the Atlantic to the Pacific Ocean, while the budget is closed by an equal freshwater transport in the opposite direction in the ocean.

In the model version before summer 2009 with the "old world" setup, this flux through the BS was damped by to the semi-closed BS. The surplus of saline water in the North Atlantic Ocean stabilized the Atlantic MOC and lead to an overturning circulation of 13.86 Sv (Sverdrup; 1 Sv = $10^6 \mathrm{m}^3\mathrm{s}^{-1}$)(Tab. 3.2). With the opening of the BS to advective flow in the "new world" setting, an increased exchange of freshwater from the Pacific Ocean through the BS to the Atlantic Ocean can take place. However, when running the ocean model under MBC, the atmospheric correction flux of vapor in the opposite direction in the atmosphere cannot take

	No Atlantic-to-Pacific correction	Atlantic-to-Pacific correction
"old world"	13.86 Sv	18.21 Sv
"new world"	2.04 Sv	14.68 Sv

Table 3.2: Maximum annual mean values of the Atlantic overturning using "old world" and "new world" with and without Atlantic-to-Pacific freshwater correction of 0.15 Sv.

place.

This absence of an atmospheric balance with an open BS leads to an excessive freshening of the North Atlantic Ocean and eventually to a shutdown of the MOC (Tab. 3.2). To avoid this effect, which is clearly inconsistent with the present-day state of the deep circulation in the North Atlantic, an artificial freshwater flux from the Atlantic to the Pacific Ocean is implemented in the model. The correction takes 0.15 Sv of freshwater from every surface box in the Atlantic basin and distributes it to the entire Pacific (Fig. 3.4). Note that this flux was not necessary when the model was run with the "old world" since a reasonably strong overturning circulation was obtained without it (Tab. 3.2). Fig. 3.5 shows the effect of the freshwater correction on the streamfunction of the overturning circulation. When applying the freshwater correction for the "old world", the MOC increases significantly in strength an depth (c). When applying no freshwater correction in the "new world", the MOC is in a complete shutdown state (b) and even with a correction flux of 0.15 Sv, the MOC is still slightly too weak (d) compared to data-based estimates of *Ganachaud and Wunsch* [2000].

Chapter 4

Model Spinup and Steady State

Only when beginning model experiments from a steady-state, useful results can be derived from perturbation simulations. With a physical spinup, the model is brought to a steady state. Due to the different fluxes through the straits, an individual model spinup needs to be calculated for every world setting described in section 3.3. In the first part of this chapter, the model spinup is described. The different steady states will be discussed in the second part of this chapter. Note that from here on, the "old world" will no longer be used. The steady state of the "old world" and further model results are described in detail in *Ritz* [2007].

4.1 Spinup

The spinup process starts with a 10,000 year calculation under RBC (equations 3.8 and 3.9). This physical spinup has restored fluxes for sea surface salinity (SSS) and sea surface temperature (SST) and brings the model to a first equilibrium. In a second step, a 1,000 year run is performed where the seasonally averaged salt flux is defined as described in section 3.4. Finally, the model is switched from RBC to MBC (equations 3.10 and 3.11) and run for another 10,000 years with MBC. At the end of this 21,000 year spinup process, the model is in the final steady state with pre-industrial temperature and salinity values.

The time series of the Atlantic and Pacific MOC in Fig. 4.1 give a first impression on the ocean circulations when running the model for 10,000 years under MBC. Positive values of the overturning in the Atlantic (Fig. 4.1a) indicate how strongly the water sinks in the regions of deep water formation. Negative values in the Pacific (Fig. 4.1b) indicate the strength of upwelling. The first 4,000 years of the time series in both Figs. show strong fluctuations in the MOC indicating the adjustment of the model to the diagnosed fluxes. Thereafter, the four time series reach their individual steady state. However, the time series of the "world BS closed" shows several periods of strong fluctuations in the MOC of over 3 Sv in the Atlantic (Fig. 4.1b), even though the model should already be in a steady state. This might indicate a possible instability of the "world BS closed" setting or a shift in the location of the maximum overturning.

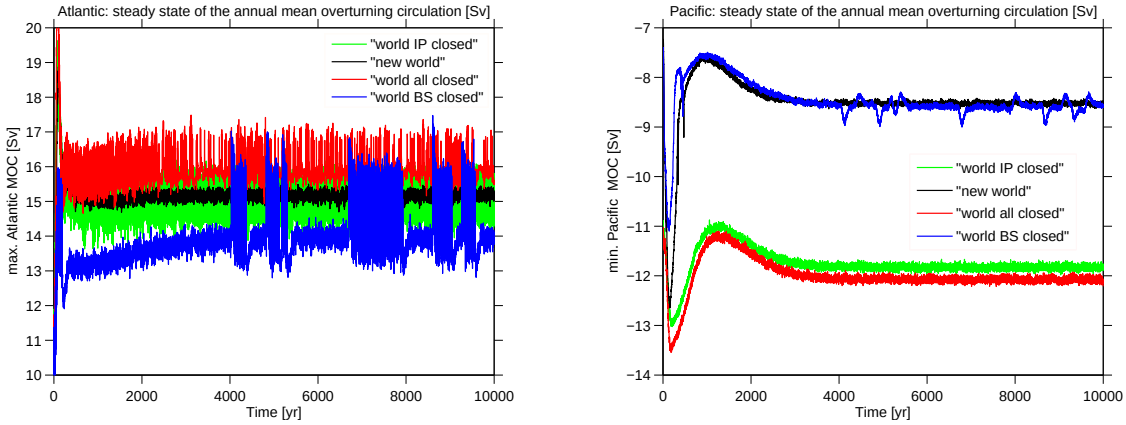

Figure 4.1: a) Annual mean values of the maximum Atlantic overturning circulation when running the model under MBC. Due to the very similar variance of the values, the time series of the "new world" was filtered with a 5-year running mean to distinguish it from the time series of the "world IP closed". b) Annual mean values of the maximum overturning circulation in the Pacific.

4.2 Steady states of the different world settings

In this section the pre-industrial steady state for all settings are discussed in detail. Note that all further model simulations in this thesis will start from the steady state described in this section.

4.2.1 Overturning circulation

While Fig. 4.1 only show the time series of the MOC in the Atlantic and Pacific, Fig. 4.2 displays the zonally averaged MOC. The strength of the overturning circulation is represented by the overturning streamfunction Ψ. The values of Ψ (in Sv) are located at the edges of every box and indicate the amount of water that flows around this point. Lines of constant streamfunction are called streamlines. Positive values of Ψ represent a clockwise circulation, negative values stand for anticlockwise circulation.

The strength of the different overturning circulations in the Atlantic and the Pacific are not the same for every setup. Depending on the fluxes through the straits, the distribution of the water masses in the ocean basins is different. In the North Atlantic, a strong overturning indicates more saline water and therefore a faster sinking of the water. In all four settings in Fig. 4.2, the surface flow to the North and the sinking of the water around 60°N is simulated, as well as the southward flow of intermediate waters and the deep overturning below 2500 m. However, the strength of the circulation and the location of the maximum overturning is different for the four world settings. The lowest values of Ψ is found for the "world BS closed" (Fig. 4.2c), which correspond to the values of the MOC in the time series in Fig. 4.1a. In the "world BS closed" setting (Fig. 4.2c), the water starts to sink slightly more to the south. This might indicate convection south of Greenland in addition to the deep water formation regions shown in Fig. 3.2. In general, the magnitude of the overturning circulation in the Atlantic represents the data-based value of 15 ± 2 Sv by *Ganachaud and Wunsch* [2000] quite well. However, the amount of North Atlantic Deep Water (NADW) which is transported over the equator are too low in all settings compared to the data-based estimates of 17 Sv by

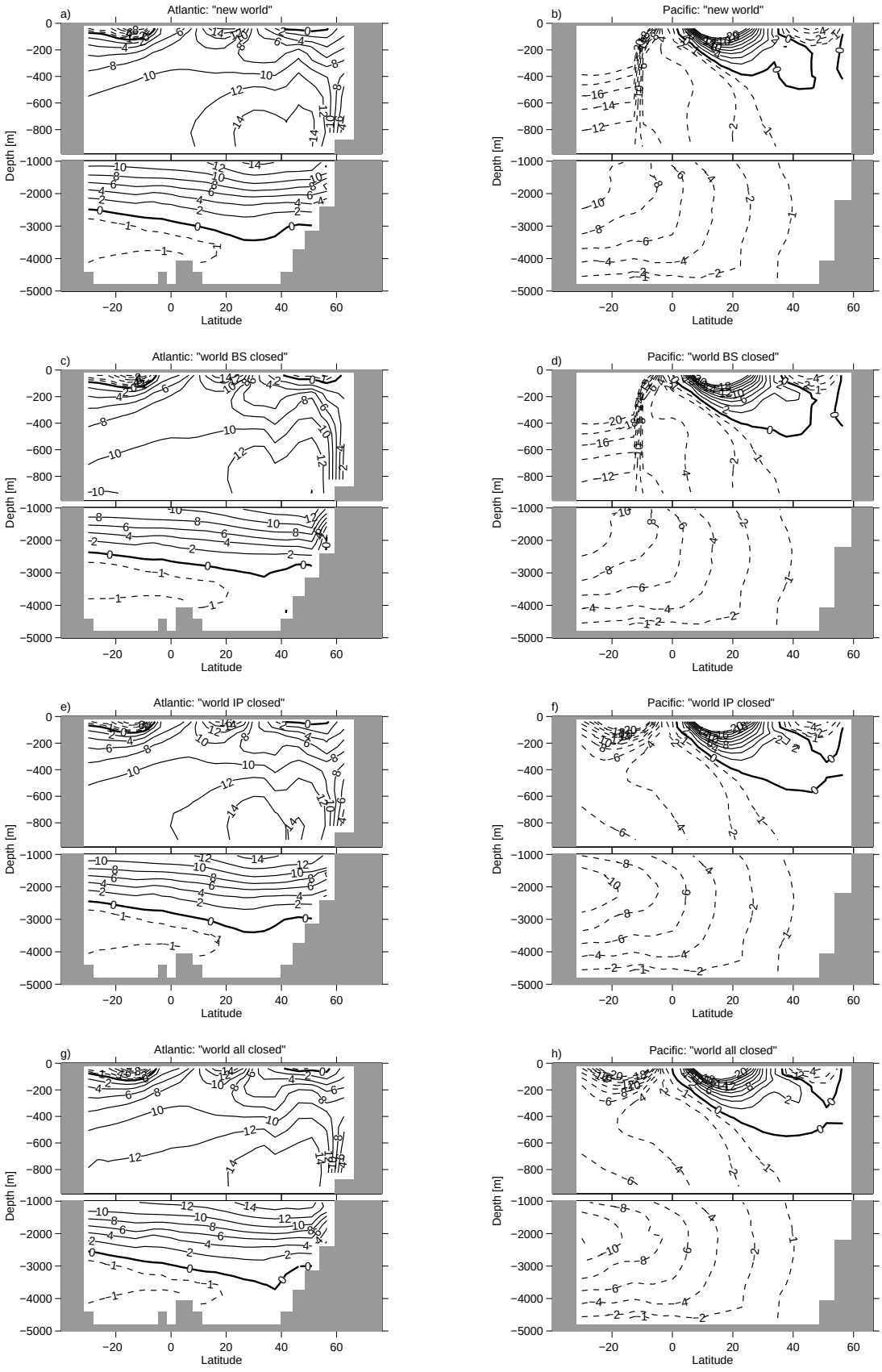

Figure 4.2: Atlantic and Pacific annual mean overturning streamfunction [Sv] of the four different world settings in a pre-industrial steady state. Positive values indicate a clockwise circulation, negative values an anticlockwise circulation.

Ganachaud and Wunsch [2000].

When comparing the overturning streamfunctions in the Pacific in Fig. 4.2, two main patterns are found. The narrow streamlines at 10°S above 800 m indicate the open IP. In a closed ocean basin, the continents form the boundaries for calculating the averaged streamfunction over the ocean basin. When the IP is open and these boundaries are missing, the averaged overturning streamfunction at this latitude is calculated wrongly. However, when comparing the four Pacific overturning patterns at the equator, similar upwelling values of almost 6 Sv can be seen in all four settings.

The problem with the missing boundaries at the IP in the "new world" (4.2b) and "world BS closed" (4.2d) also arises when comparing the maximum values of the Atlantic MOC in Fig. 4.1a. The Pacific minimum overturning of these two settings is about 3.5 Sv lower compared with the other two setups. To calculate the annual mean minimum overturning in the Pacific, the model searches only in the boxes which satisfy the boundary conditions, i.e., in the closed basin. For the setups with closed IP, the model searches for the minimum value from 38°S and 63°N, whereas the minimum value in the case of an open IP can only be located between 10°S to 63°N. Note that due to this boundary problem, time series of different world settings of the Pacific can only be compared with caution.

4.2.2 Salinity and Convection

The distribution of salinity in the ocean has a major impact on convection and therefore on the overturning circulation. The concentration of salinity in the Atlantic is higher than in the Pacific at the same latitude. This is due to the patterns of water vapor transport in the atmosphere [*Zaucker and Broecker*, 1992]. The Pacific, Arctic and Southern Ocean are net precipitation basins, which means that the evaporation is smaller than the precipitation. This results in rather low SSS. In contrast, high SSS values are found in the net evaporation basins, where the evaporation of ocean water is higher than the precipitation [*Talley*, 2008]. Most of the atmospheric water vapor is transported from the Atlantic to the Pacific, resulting in large salinity difference between these two basins [*Talley*, 2008]. The strong insulation in the Subtropics leads to high SSS between 30°N and 30°S. The shallow bathymetry and the insufficient of exchange with the Atlantic lead to a very saline Mediterranean Sea.

Global mean annual SSS for the four world settings can be seen in Fig. 4.3a-d. The open BS leads to an inflow of fresher water from the Pacific into the Atlantic and therefore to lower salinity in the Labrador Sea in the "new world" and "world IP closed" setup (Fig. 4.3a and c). Because the BS is closed in the "world all closed" slightly higher SSS values can be observed for this setting (d). In general, the three setups have a very similar distribution of SSS in the steady state. Interestingly, the "world BS closed" (Fig. 4.3b) has very high SSS in the Labrador Sea but rather low salinity values in the GIN Sea. Even one box of fresh water can be seen east of Greenland. By comparing the SSS values with the convection frequencies shown in Fig. 4.3e-h, a similar pattern can be seen again for the "new world", the "world IP closed" and the "world all closed". The main region of convection is in the two columns in the GIN Sea, while almost no convection takes place south of Greenland. However, for the "world BS closed" a distinct convection pattern can be observed. Due to the fresh column in the GIN Sea, no convection takes place in this region, but only south of Greenland and south of the Labrador Sea (Fig. 4.3b and f). The absence of convection in the region of deep

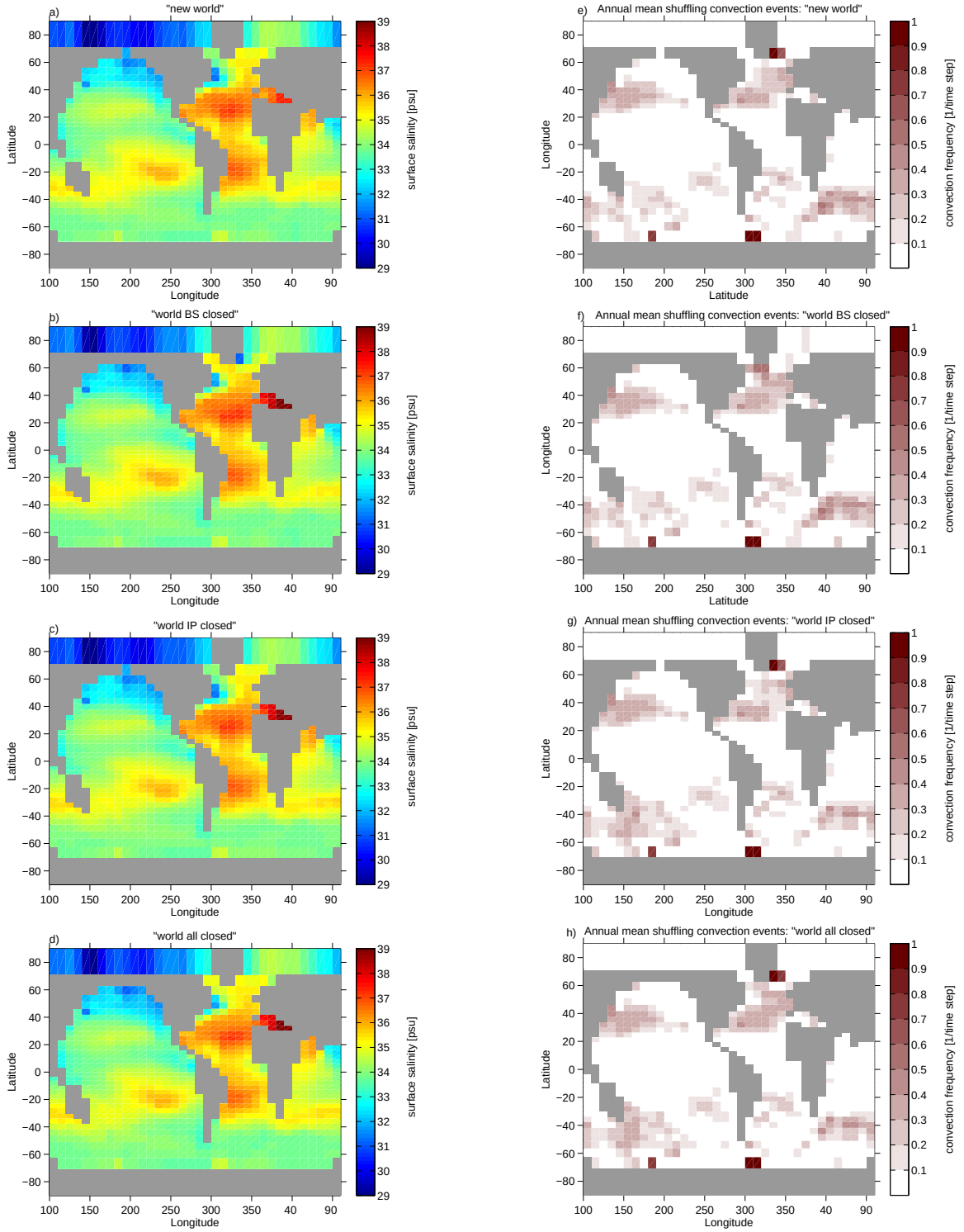

Figure 4.3: Global annual mean SSS fields [psu] (a-d) and annual mean shuffling convection frequency (e-h) of the four world setups in the pre-industrial steady state. A convection frequency of 1 indicates shuffling convection at every time step.

water formation seems to be the case for the rather low overturning circulation for this world setting (see Fig. 4.1a).

Global mean annual SSS for the four world settings can be seen in Fig. 4.3a-d. The open BS leads to an inflow of fresher water from the Pacific into the Atlantic and therefore to lower salinity in the Labrador Sea in the "new world" and "world IP closed" setup (Fig. 4.3a and c). Because the BS is closed in the "world all closed" slightly higher SSS values can be observed for this setting (d). In general, the three setups have a very similar distribution of SSS in the steady state. Interestingly, the "world BS closed" (Fig. 4.3b) has very high SSS in the Labrador Sea but rather low salinity values in the GIN Sea. Even one box of fresh water can be seen east of Greenland. By comparing the SSS values with the convection frequencies shown in Fig. 4.3e-h, a similar pattern can be seen again for the "new world", the "world IP closed" and the "world all closed". The main region of convection is in the two columns in the GIN Sea, while almost no convection takes place south of Greenland. However, for the "world BS closed" a distinct convection pattern can be observed. Due to the fresh column in the GIN Sea, no convection takes place in this region, but only south of Greenland and south of the Labrador Sea (Fig. 4.3b and f). The absence of convection in the region of deep water formation seems to be the case for the rather low overturning circulation for this world setting (see Fig. 4.1a).

In addition to the surface salinity, a depth-profile of the salt distribution is shown in Fig. 4.5. The path goes from 63°S/165°W through the Pacific, Arctic Ocean and Atlantic to 63°S/25°W and is marked blue in Fig. 4.4. The column of fresh water in the "world BS closed" east of Greenland (at 63°N in Fig. 4.5b) is only three boxes deep, but as seen in Fig. 4.3f, this seems to be enough to cause a shift of the convection cell. In both cases with a closed BS, the Arctic Ocean is more saline at depth, since no mixing with fresh water from the Pacific can take place. The high salinity in the subtropical Atlantic Ocean is evident in all the settings, however the ocean north of the equator is saltier than south, which corresponds also to the SSS in Fig. 4.3. Especially the high salinity in depth could be explained by to the inflow of highly saline water from the Mediterranean Ocean at 35°N, because the rather low SSS values in Fig. 4.3a correspond well with the lack of salinity below 800 m in Fig. 4.5a.

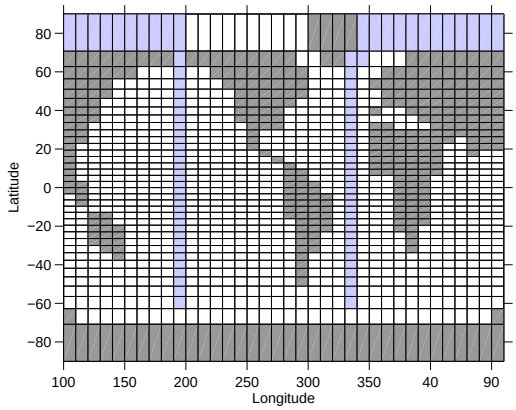

Figure 4.4: The blue boxes represent the path for the salinity profile shown in Fig. 4.5.

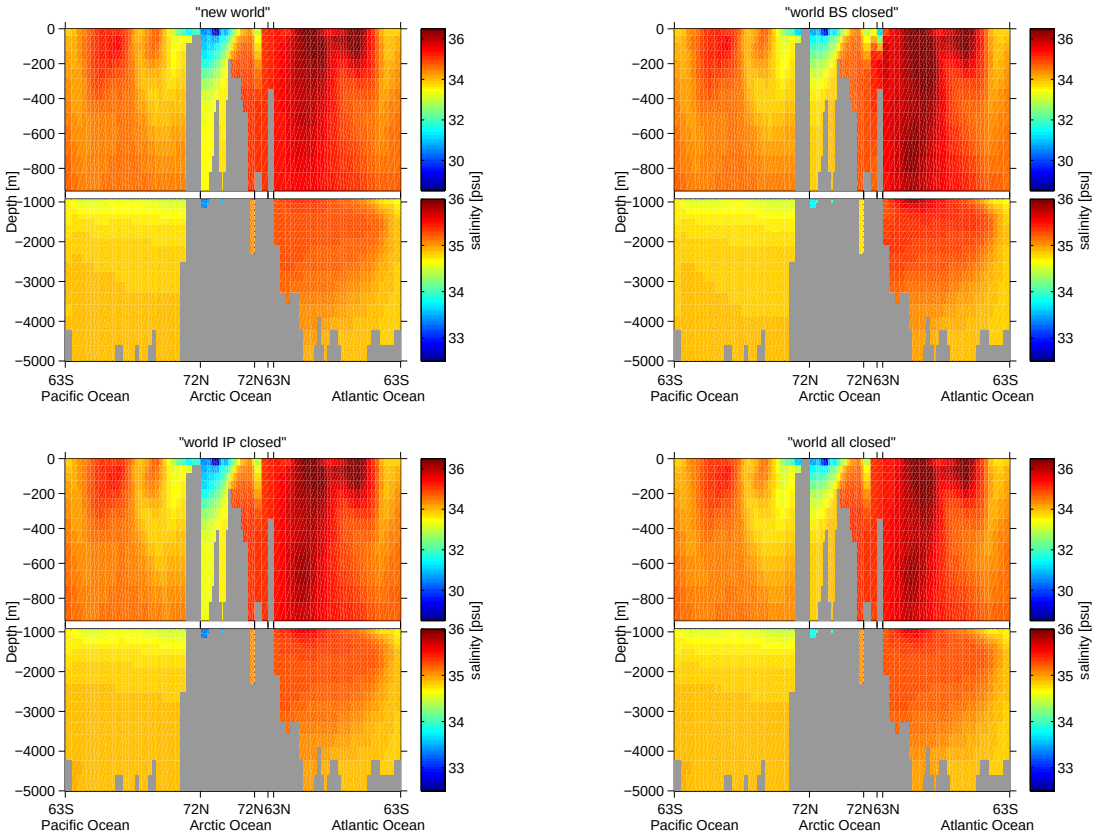

Figure 4.5: Depth-profile of salinity for the four world settings in steady state. The path for the profile is shown in Fig. 4.4. Note that a different colorbar is used below 1,000 meters.

The three settings with high SSS in the Mediterranean Sea have high salinity to a depth of 1,000 m.

4.2.3 Barotropic streamfunction

The mostly wind-driven surface gyre circulations are quantified by the barotropic streamfunction (in Sv, Fig. 4.6). Again, positive values indicate a clockwise circulation while negative values stand for an anticlockwise circulation. Overall, most surface gyres in the model are underestimated compared to the data-based values by *Ganachaud and Wunsch* [2000], even though the wind stress has been doubled compared to the data-based estimates of *Kalnay et al.* [1996] to strengthen the circulations. The Antarctic circumpolar current (ACC), for example, has a transport of 140 Sv through the Drake Passage (DP) according to *Ganachaud and Wunsch* [2000], while in our model the average transport around Antarctica is only about 45 Sv. Also the subtropical gyre (10°N and 45°N) and the subpolar gyre (45°N to 60°N) are too weak compared to data-based estimates by *Bacon* [1997] and *Read* [2000].

The opening of the BS and the IP allows barotropic flow through the two passages. In the "new world", 1 Sv flows northward through the BS and 21 Sv pass through the opening between Australia and Indonesia. These fluxes correspond quite well to measured values of *Ganachaud and Wunsch* [2000] who estimate 1 Sv for the BS and 16 $\pm$ 5 for the IP. When

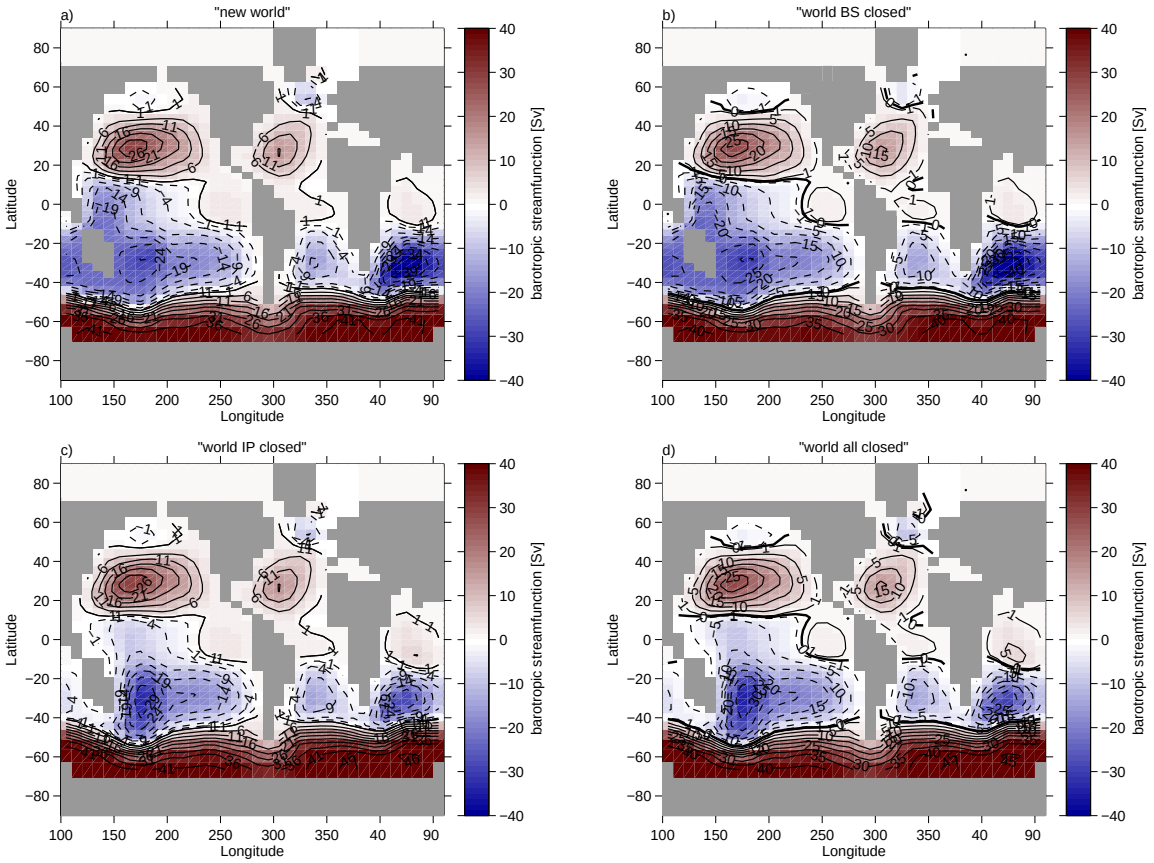

Figure 4.6: Annual mean barotropic streamfunction [Sv] of the four world settings in the pre-industrial steady state. Positive values indicate a clockwise circulation, negative values counter clockwise water transport.

the IP is closed, the center of the gyre in the South Pacific is located east of Australia. As no water can pass through the IP, the gyre in the Indian Ocean is weaker in these two settings compared to the one with open IP.

Chapter 5

Freshwater Experiments in the Bern3D Model

5.1 Motivation

Proxy records from ice cores and sediments show a number of abrupt changes of the climate during the last glacial period, e.g., *Stocker* [2000] (see section 2.2). Many of the abrupt cooling events (e.g., the Younger Dryas) are suggested to be triggered by freshwater input into the North Atlantic, followed by a significant reduction or even a shutdown of the NADW formation and thus the overturning circulation. To gain insights in the mechanism of such events an appropriate tool is to perturb ocean models with freshwater in the North Atlantic.

The model response to freshwater perturbations and the amount of freshwater which is needed to cause a complete shut down of the Atlantic MOC is not the same for every ocean model. It is therefore important to test the sensitivity of the Bern3D ocean model to positive and negative freshwater perturbations in the North Atlantic.

This chapter presents a number of freshwater perturbation experiments and discusses the impact of freshwater on the MOC in the Bern3D model. In *Ritz* [2007], perturbation experiments are described using the "old world". Two equilibrium states of the Atlantic MOC were found, i.e., the circulation was either in an "on" or an "off" state, but no equilibrium state in between was identified. For this thesis, similar experiments were done as by *Ritz* [2007], however with the "new world". The goal is to test the sensitivity of the new setting to freshwater perturbations and to see whether different equilibria of the MOC can be achieved when the BS and the IP are open.

5.2 Different states of the MOC

For all the experiments described in this work, freshwater was injected in the region from 45-70°N in the Atlantic (Fig. 5.1). It is the typical perturbation region for freshwater experiments and this input region was also used in the study by *Ritz* [2007]. The duration of the injection perturbation was varied between 1,000 and 2,000 years and the shape of the pulse was chosen to be either rectangular or triangular.

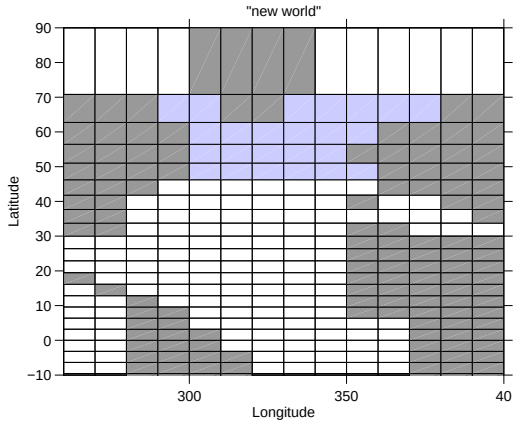

Figure 5.1: Input region of the freshwater experiments described in this work (45-70°N).

In a first set of seven perturbation experiments, the reaction of the Atlantic MOC to different freshwater forcings was tested. A summary of the seven runs is found in Tab. 5.1. The freshwater perturbation in all seven experiments had a duration of 1000 years and the pulse had a rectangular shape, i.e., the maximum freshwater amount was injected for the whole period of the perturbation.

Fig. 5.2 displays the time series of the annual mean maximum Atlantic MOC. Note that the values displayed have been filtered with a 5-year running mean in order to reduce the high-frequency variability. Three equilibrium states are found, but also the recovery times of the MOC differ from experiment to experiment. After perturbing the model, all experiments, except for the one which shows oscillations, show a rapid decrease of the MOC from about 15 Sv to about 8 Sv. The overturning circulation of the experiments SD, SR1, SR2 and SR3 decreases further to about 1 Sv, though with different slopes. Only the run SD stays at an off state of the MOC. All the other runs eventually recover to an intermediate equilibrium between 11.5 Sv and 12.5 Sv. Due to the weak perturbations, the MOC of the runs WK1 and WK2 never shuts down completely and remains at the intermediate equilibrium after the perturbation.

Name of experiment	max. freshwater amount	Name of equilibrium state
OSC	0.02 Sv	steady “on” state
WK1	0.05 Sv	steady “intermediate” state
WK2	0.07 Sv	steady “intermediate” state
SR1	0.08 Sv	steady “intermediate” state
SR2	0.09 Sv	steady “intermediate” state
SR3	0.10 Sv	steady “intermediate” state
SD	0.11 Sv	steady “off” state

Table 5.1: Setup of the seven freshwater experiments and the equilibrium state at the end of the run (year 7,000 in Fig. 5.2).

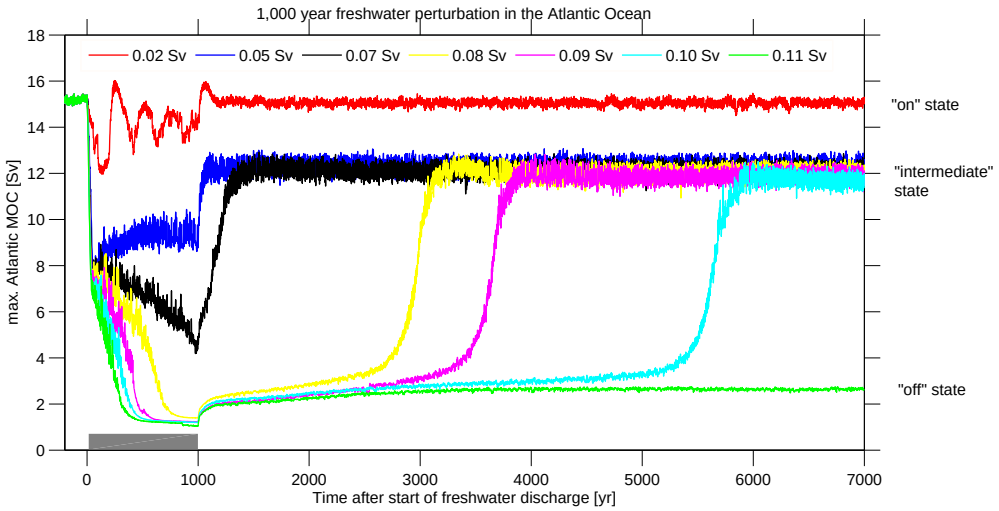

Figure 5.2: Time series of the annual mean max. Atlantic MOC when applying different freshwater pulses during 1,000 years. In order to reduce the high frequency variability, the time series was filtered with a 5-year running mean. The three equilibrium states at the year 7,000 are called steady "on" state, steady "intermediate" state and steady "off" state. The gray bar indicates the freshwater perturbation.

Interestingly, the circulation of the run OSC is very different. After the freshwater discharge, a reduction of the MOC is observed, however it is not as rapid as in the other six experiments. After about 150 years, the MOC recovers and starts to oscillate for the duration of the freshwater perturbation. The oscillation has a slightly damped amplitude with a minimum value of 12 Sv at year 150 and a maximum of 16 Sv at year 270. The average period of these oscillations is At the end of the perturbation, the MOC overshoots slightly before the circulation returns to the normal steady state. Oscillations in the MOC due to freshwater perturbations have not been observed in previous experiments with the "old world". Therefore, the assumption can be made that the opening of the IP and BS have an impact on the dynamics in the ocean which can cause these instabilities of the MOC after freshwater perturbations. In chapter 6 the oscillations and their possible origin are discussed in detail.

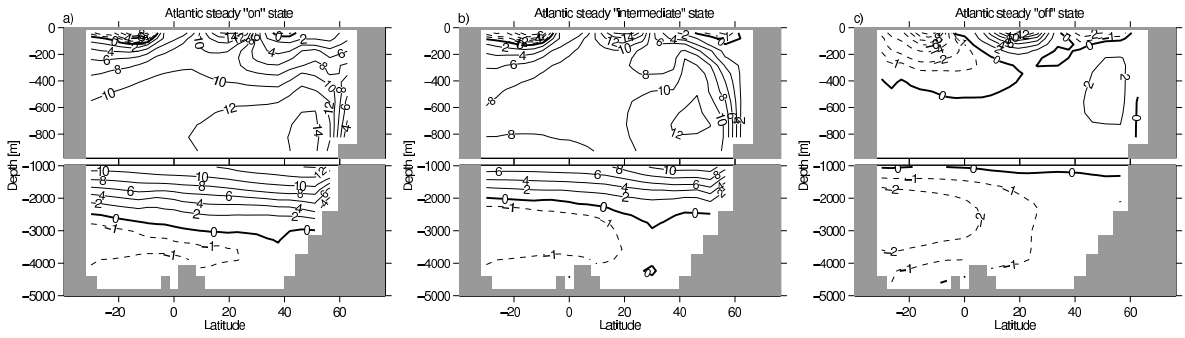

Figure 5.3: Annual mean overturning streamfunction [Sv] of the three equilibrium state of the Atlantic MOC: a) Atlantic steady "on" state, b) Atlantic steady "intermediate" state and c) Atlantic steady "off" state.

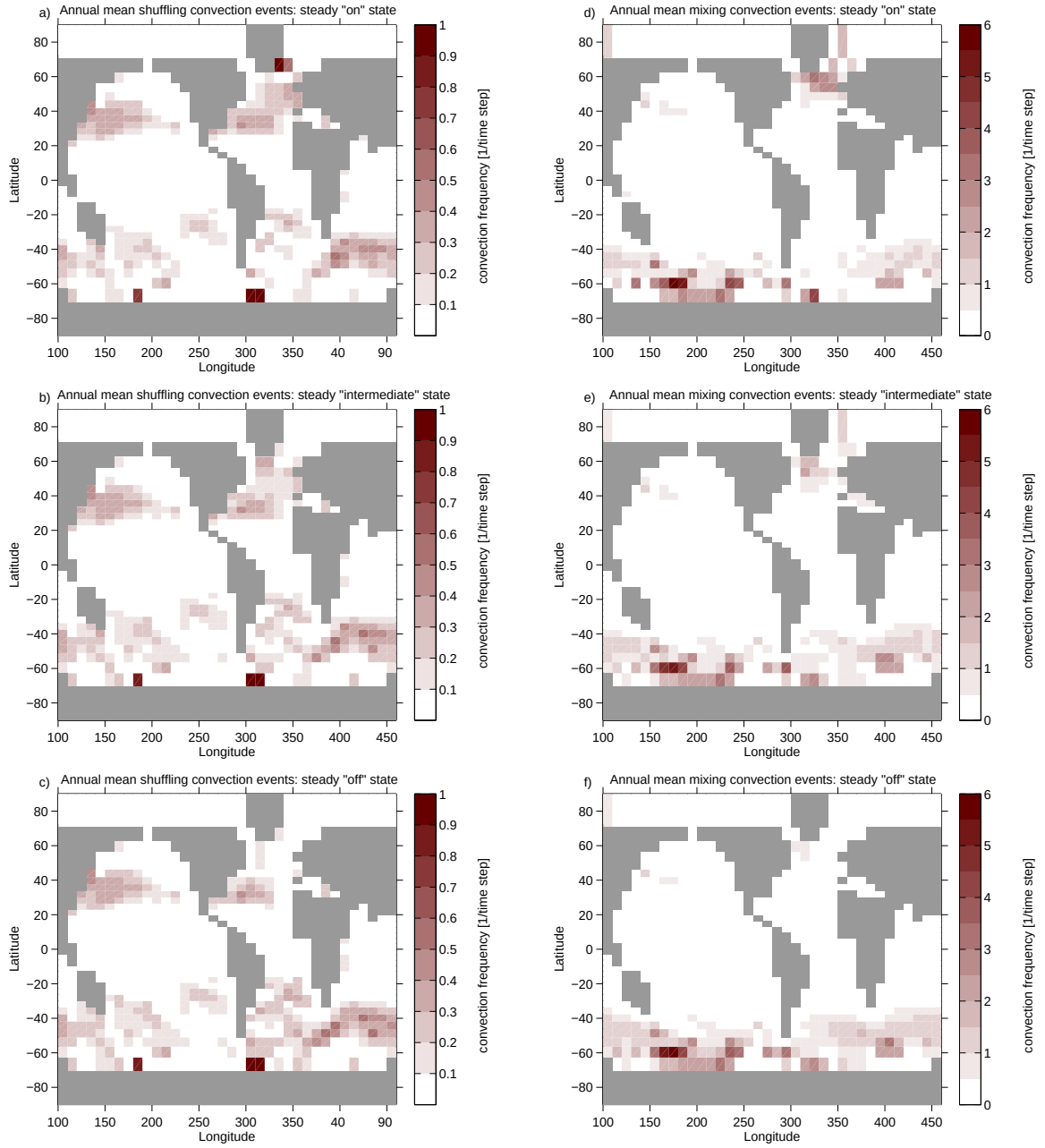

Figure 5.4: Annual mean mixing (a-c) and shuffling (d-f) convection of the three equilibrium state of the Atlantic MOC. A frequency of 1 in the shuffling convection indicates shuffling convection for every time step. Mixing convection can have more than one convection event between different layers per time step.

The three equilibrium states are called steady “on”state, steady “intermediate”state and steady “off”state (see Tab. 5.1). Fig. 5.4 shows the global annual mean shuffling and mixing convection of the three equilibriums and in Fig. 5.3 the corresponding annual mean overturning circulations is shown. In the steady “on” state, the strong shuffling convection in the GIN Sea, which reaches almost to the ocean depth, is the main driver for the stable overturning. The mixing convection is also very pronounced in the North Atlantic, however the strongest

mixing takes place south of Greenland. Note that the overturning in the "on" state (Fig. 5.3a) is the same as discussed in section 4.2.1. In the "intermediate" and the "off" state, the shuffling convection east of Greenland has significantly ceased. However, a region with shuffling convection south of Greenland has developed in the "intermediate" state, with a convection depth of about 500 meters. This might be the driver for the still quite strong MOC, even though the convection in the deep water formation region has shut down. The slight shifting of the location of maximum overturning in Fig. 5.3b also indicates the different location and the reduced strength of the convection. In the "off" state, both the mixing and the shuffling convection have ceased, leading to the total shutdown of the MOC. The southward flow of the NADW is only very weak and above 1,000 m, while the strength of the AABW is increased (Fig. 5.3c).

5.3 Negative freshwater forcing

Since the MOC does not recover on its own from the steady "off" state to the "on" state but only to the "intermediate" state when the model is run with MBC, the model has to be forced back to the original circulation. This can be achieved by applying a negative freshwater forcing, i.e., by adding salt into the North Atlantic.

To investigate the model response to a negative perturbation, the run SD is used as a basis for the experiment. After a freshwater perturbation of 0.11 Sv during 1,000 years, a negative pulse of the same magnitude and duration is applied. The simulation is called REC1 and characteristics are given in Tab. 5.2. The time series of the maximum Atlantic MOC in Fig. 5.5 shows a shutdown of the overturning during the freshwater pulse. When the negative perturbation starts at year 1,000, the MOC recovers abruptly, and stays at a high level of almost 18 Sv until the end of the perturbation. The circulation does not reach the steady "on" state after the end of the negative freshwater discharge, but decreases its strength to 12.5 Sv, which corresponds to the overturning of the steady "intermediate" state.

The experiment was repeated with the same parameter setup, however with a triangular shape of the freshwater pulse (Tab. 5.2) to test whether the MOC can be brought back to the initial steady state. This second experiment is called REC2. As can be seen in Fig. 5.6, the Atlantic MOC reduces the strength slower after the start of the freshwater discharge since the model has more time to adapt to the forcing when using a triangular shape of the pulse. The minimum of the overturning circulation is reached only about 500 years after the peak of freshwater discharge. Also the recovery of the MOC is slower compared to the experiment

Characteristic	REC1	REC2
max. positive freshwater	0.11 Sv	0.11 Sv
max. negative freshwater	– 0.11 Sv	– 0.11 Sv
duration of positive perturbation	1,000 years	1,000 years
duration of negative perturbation	1,000 years	1,000 years
shape of freshwater pulse	rectangular	**triangular**

Table 5.2: Parameter setup for the runs REC1 and REC2. Changes with respect to the run REC1 are marked bold .

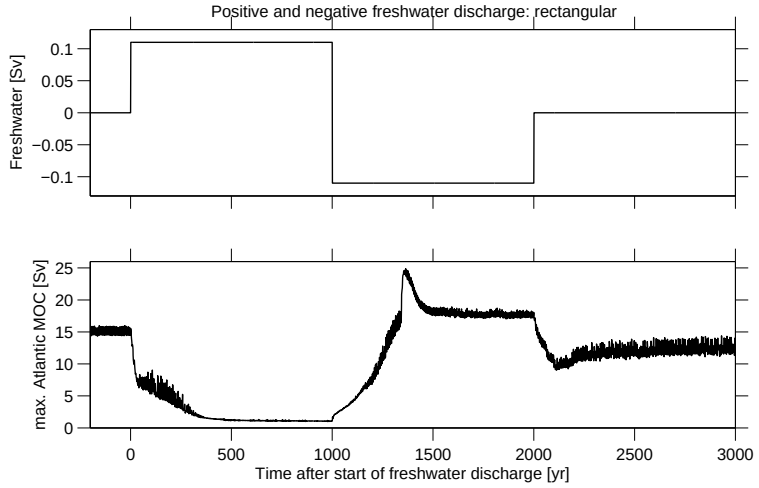

Figure 5.5: Positive and negative freshwater discharge in the Atlantic Ocean in a rectangular shape of the pulse (top) and the resulting changes in the max. Atlantic MOC in the REC1 experiment (bottom).

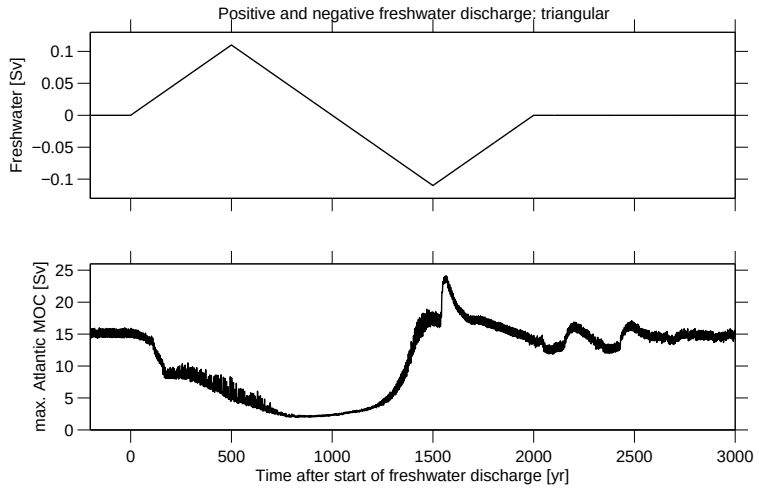

Figure 5.6: Positive and negative freshwater discharge in the Atlantic Ocean in a triangular shape of the pulse (top) and the resulting changes in the max. Atlantic MOC in the REC2 experiment (bottom).

REC1. Once the negative pulse is on its maximum, the MOC has recovered to 18 Sv, which is almost 3 Sv higher than in the steady state. As the salt input already diminishes, the MOC shoots up abruptly to a maximum of 24 Sv and only then starts to decrease. After the perturbation, the MOC oscillates with a frequency of about 250 years for almost 1,000 years, but finally the REC2 run eventually ends in the "on" state.

A zoom on the recovery and the overshoot of the MOC of the run REC2 can be seen in Fig. 5.7. In order to explain the rapid strengthening of the overturning circulation, which leads to the overshoot, the shuffling convection of the four periods in time labeled with a red circles is compared in Fig. 5.8. As the MOC starts to recover (Fig. 5.8a), convection can be observed south of Greenland. It increases steadily as the MOC gains in strength (Fig.

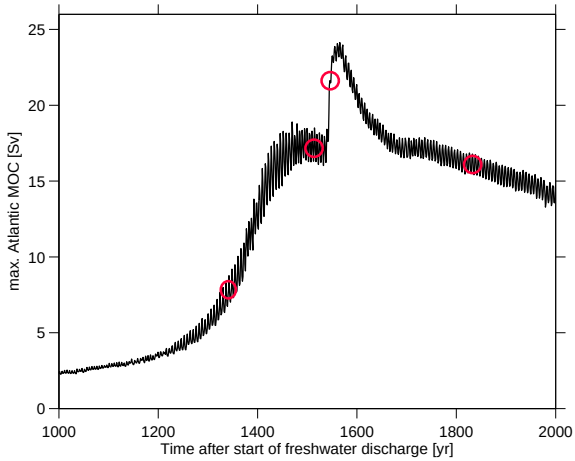

Figure 5.7: Zoom on the Atlantic MOC during the 1,000 year of negative freshwater forcing in the run REC2. The red circles indicate the three periods in time where the shuffling convection is analyzed.

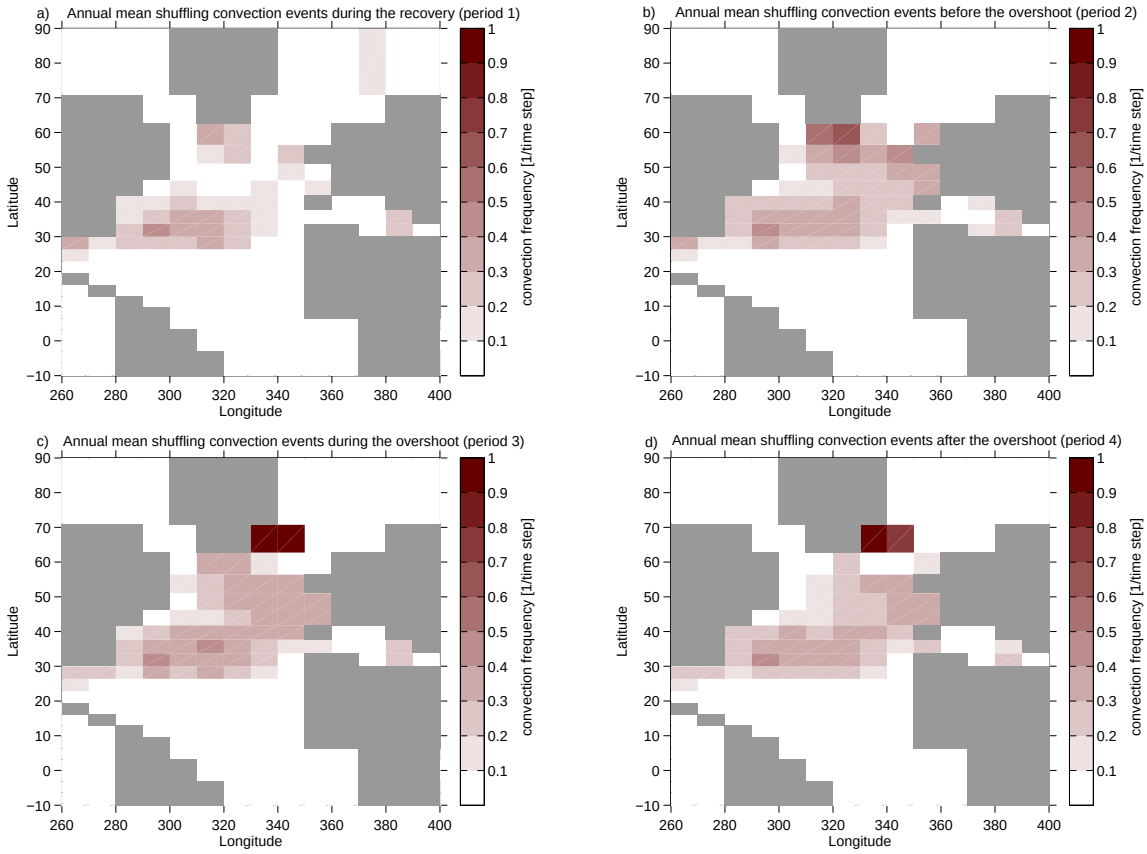

Figure 5.8: Annual mean shuffling convection in the North Atlantic during four stages of the Atlantic MOC recovery: a) when the MOC starts to recover, b) at the threshold before the overshoot, c) during the overshoot of the MOC and d) after the overshoot.

Characteristic	REC3	REC4
max. positive freshwater	0.11 Sv	0.11 Sv
max. negative freshwater	-0.11 Sv	-0.11 Sv
duration of positive perturbation	**2,000 years**	**2,000 years**
duration of negative perturbation	**2,000 years**	**2,000 years**
shape of freshwater pulse	rectangular	**triangular**

Table 5.3: Parameter setup for the runs REC3 and REC4. Changes with respect to the run REC1 are marked bold.

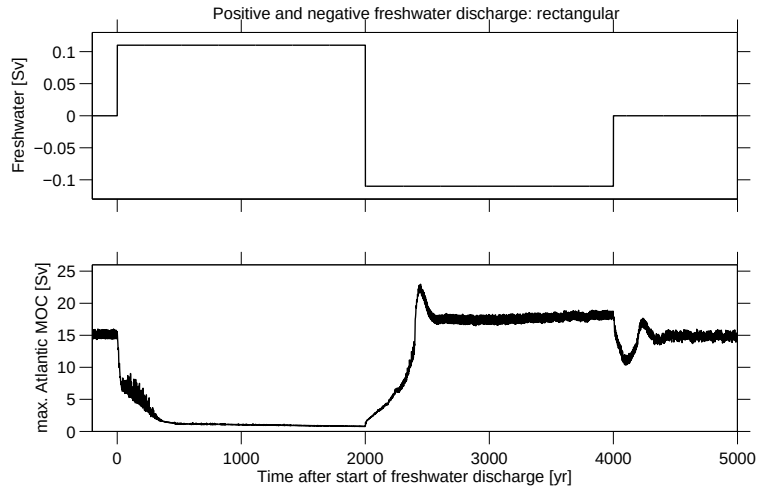

Figure 5.9: Positive and negative freshwater discharge in the Atlantic Ocean in a rectangular shape of the pulse (top) and the resulting changes in the max. Atlantic MOC in the REC3 experiment (bottom).

5.8b). The overall convection pattern of the overturning circulation during the recovery is the same as in the steady "intermediate" state (see Fig. 5.4b). When a threshold of the negative perturbation is reached, additional strong convection also appears in the GIN Sea (Fig. 5.8c), leading to the drastic increase in the MOC and to the overshoot. However, the strong convection in both regions lasts only for a short period of time. After the overshoot, the convection south of Greenland decreases in strength while it stays stable in the GIN Sea. This convection pattern is the same as in the steady "on" state, which was shown in Fig. 5.4c.

Not only the shape of the pulse defines whether the MOC recovers completely, but also the duration of the perturbation. This is shown in the experiments REC3 and REC4 (Tab. 5.3) where both perturbations have a duration of 2,000 years. The longer negative pulse leads to a full recovery of the MOC in both experiments, as can be seen in Fig. 5.9 and 5.10. Interestingly, the threshold of the negative freshwater perturbation for an MOC overshoot in experiment REC4 is reached even before the negative discharge is at a maximum. Also, the oscillations which were found after the end of the negative triangular pulse in the short perturbation are not evident in the experiment with an increased duration of the freshwater forcing.

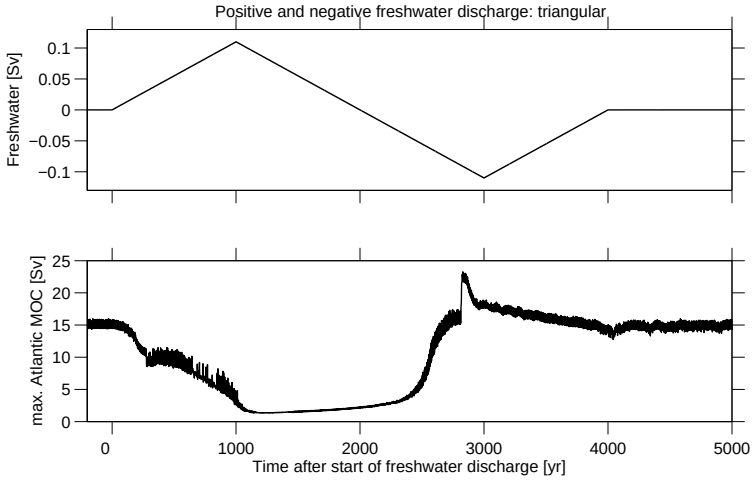

Figure 5.10: Positive and negative freshwater discharge in the Atlantic Ocean in a rectangular shape of the pulse (top) and the resulting changes in the max. Atlantic MOC in the REC4 experiment (bottom).

5.4 MOC Hysteresis

In a number of early studies with ocean models, it was shown that the ocean-atmosphere system has more than one stable mode of operation [*Stocker and Wright*, 1991; *Stocker and Marchal*, 2000; *Rahmstorf et al.*, 2005]. It is suggested that the ocean has a hysteresis behavior, very like other non-linear physical systems. This implies that more than one stable state can be achieved for the same control variable. For our freshwater experiments, this means that after a positive perturbation, the Atlantic MOC does not necessarily go back to the initial

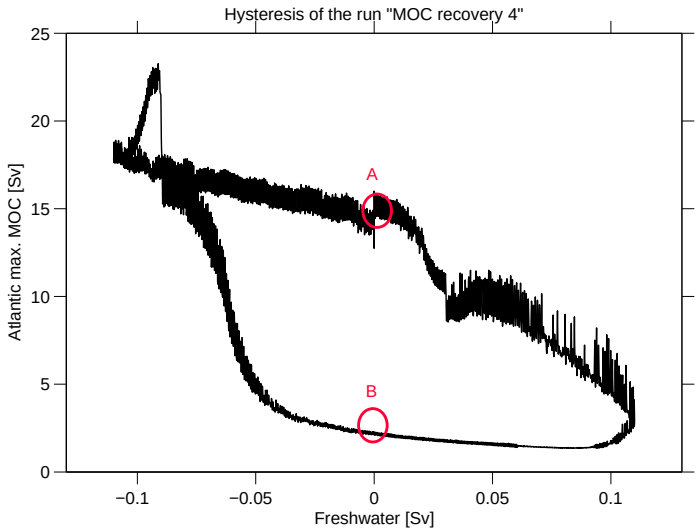

Figure 5.11: Max. Atlantic MOC [Sv] plotted against the freshwater forcing [Sv] applied in the North Atlantic for the run REC4. The two equilibrium states of the MOC are marked by the red circles.

steady state but can adjust to another steady state after the end of the perturbation.

The hysteresis behavior of the model is shown in Fig. 5.11, which displays the Atlantic MOC of the run REC4 plotted against the positive and the negative freshwater forcing. Note that in order to produce a hysteresis, the shape of the perturbation has to be triangular, because only a continuous rise in the forcing and a slow adaptation of the circulation can be nicely displayed. Two equilibrium states (labeled with red circles) can be seen where the MOC is either in the "on" or in the "off" state. The path of the hysteresis starts from equilibrium **A**. The decrease in the MOC as the freshwater is perturbed can be nicely observed. When the Atlantic Ocean is too fresh after the perturbation, the MOC has come to a complete shutdown and remains in equilibrium **B**. A negative perturbation is needed to increase the circulation and finally reach the initial equilibrium a again. Also the overshoot in the MOC shortly before the maximum of the negative perturbation is evident.

Chapter 6

Oscillations in the Atlantic MOC during Freshwater Experiments

6.1 Motivation

In the Bern3D model, oscillations of the Atlantic MOC in freshwater experiments, as in the previous chapter, are not found when the IP and the BS are closed in the "old world". As they only occur with the "new world", it is very likely that they are linked to instabilities in the model caused by the opening of the two straits.

In the literature, a number of studies discuss the appearance of oscillations in the Atlantic MOC during freshwater perturbations [*Yoshimori et al.*, 2010; *Schulz et al.*, 2006; *Knutti and Stocker*, 2002]. However, the frequency and the overall characteristics of the oscillations is strongly model dependent. Also the origin is usually not easy to detect and a number of processes related to their appearance is suggested. On the one hand, oscillations can result when the MOC is close to a threshold, where only small changes of the freshwater flux can cause rapid changes in the MOC. The quantification of such thresholds is very difficult and is in many cases unknown [*Knutti and Stocker*, 2002]. Also an interplay of oceanic and atmospheric feedbacks can lead to instabilities and oscillations in the MOC as it is shown in the study by *Yoshimori et al.* [2010]. *Schulz et al.* [2006] showed that a periodic change between deep water formation in the GIN Sea and in the Labrador Sea can lead to the appearance of oscillations in model the output. However, since such mechanisms are strongly dependent on the type and the resolution of the model in question, a generalization is not possible.

In order to identify the origin of oscillations in our model, it is important to understand their characteristics. Only by doing this, it is possible to make a link to physical feedbacks related to oscillations. However, it may also be possible that the oscillations occur due to numerical instabilities in the model. Numerical problems should be solved since they can lead to wrong model results and conclusions in future simulations.

Three world settings were newly created with either one or both straits closed as described in section 3.3. The goal is to understand the effects of the fluxes through the straits on the behavior of the Atlantic MOC. This chapter discusses simulations with the four world masks and the occurrence of oscillations. In a first step, this is done by a sensitivity study with the

four world settings. Secondly, the characteristics of the oscillations will be described and in a last step, an attempt is made to discuss their physical and numerical origin.

6.2 Oscillations in the four world settings

In this section the effect of the opening of the IP and the BS on the appearance of oscillations in the Atlantic MOC is tested in a sensitivity study. For this, the three newly created world setting described in section 3.3 and the "new world" are used.

Studies by *Richter and Xie* [2010] and *Zaucker et al.* [1994] discuss the importance of the Atlantic-to-Pacific freshwater correction on the strength and the stability of the Atlantic MOC. When the correction flux is applied, the Atlantic MOC is strengthened due to the higher salinity in the North Atlantic. In model computations with the "new world", this correction is essential to obtain deep water formation in the North Atlantic (see section 3.7). Also, the wind stress scaling is suggested to have an influence on the strength of the MOC in model simulations [*Arzel et al.*, ; *Arzel et al.*, 2008; *Nof*, 2000], where a more stable overturning is achieved when the scaling factor is high. To analyze the effect of these two factors on the MOC in our model during freshwater experiments, a sensitivity study was performed. The goal was to investigate the effect of the Atlantic-to-Pacific correction and the wind stress scaling on the stability of the Atlantic MOC of the four world settings.

For the sensitivity experiments, either the Atlantic-to-Pacific correction or the wind stress scaling was kept constant. The other parameter was increased by 0.001 Sv and 0.001 %, respectively, in each run. Also the freshwater forcing in the North Atlantic between 50°N and 70°N was increased by 0.001 Sv. Tab. 6.1 gives an overview on the eight experimental setups. Note that the duration of the freshwater discharge was set to 1,000 years in every experiment and the shape of the pulse was rectangular.

Name of Experiment	Name of World setting	Freshwater forcing [Sv]	Freshwater correction [Sv]	Wind stress scaling factor
SENS1	"new world"	0.010 ... 0.026	0.13 ... 0.17	2.0
SENS2	"new world"	0.010 ... 0.026	0.15	1.9 ... 2.1
SENS3	"world IP closed"	0.004 ... 0.020	0.13 ... 0.17	2.0
SENS4	"world IP closed"	0.004 ... 0.020	0.15	1.9 ... 2.1
SENS5	"world all closed"	0.015 ... 0.031	0.13 ... 0.17	2.0
SENS6	"world all closed"	0.015 ... 0.031	0.15	1.9 ... 2.1
SENS7	"world BS closed"	0.080 ... 0.096	0.13 ... 0.17	2.0
SENS8	"world BS closed"	0.080 ... 0.096	0.15	1.9 ... 2.1

Table 6.1: Parameter setup for the sensitivity experiments with the four world settings. The variable parameters are different in every run. The shape of the perturbation is triangular and the duration of the discharge is 1,000 years for all the experiments.

Based on this large number of model runs (1,054 runs were performed with every world setting), a number of different oscillation patterns were found. In total, four types of responses for the evolution of the MOC could be distinguished:

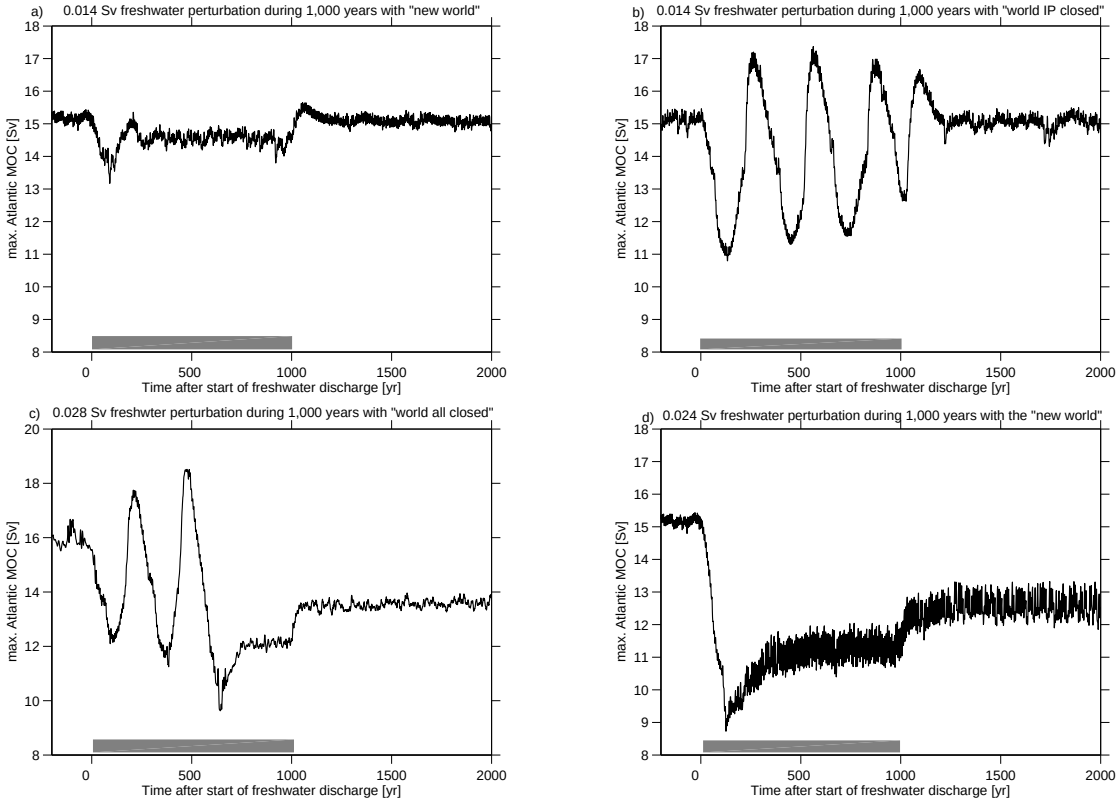

Figure 6.1: Illustration of four types of responses to perturbations. Annual mean max. Atlantic MOC during a 1,000-year freshwater discharge experiment: (a) 0.014 Sv using the "new world", (b) 0.014 Sv using the "world IP closed", (c) 0.014 Sv using the "world all closed", (d) 0.024 Sv using the "new world". The time series are filtered with a 5-year running mean. The gray bars indicate the duration of the freshwater perturbation.

- *No Oscillation*: The MOC weakens slightly for the duration of the perturbation, but does not oscillate (Fig. 6.1a).
- *Oscillation Type 1*: Oscillations in the MOC are found for the duration of the freshwater perturbation. The frequency of the oscillation varies between 200 and 250 years and the amplitude decreases with time (Fig. 6.1b).
- *Oscillation Type 2*: The MOC oscillates at the beginning of the perturbation but slows down to an intermediate level after a few hundreds of years. The amplitude of the oscillations increases with time. (Fig. 6.1c).
- *Weak MOC*: The MOC slows down instantaneously after the beginning of the perturbation to an intermediate level (Fig. 6.1d).

6.2.1 Classification scheme

In order to analyze and visualize the large number of runs performed in the sensitivity study, a classification scheme was developed using Spectral Analysis (SA). While normal time series are usually described in the *time domain* with values h as a function of time $h(t)$, spectral methods transform time series to the *frequency domain*, which displays the amplitude H as a function of frequency f, that is $H(f)$, with $-\infty < f < \infty$ [*Press et al.*, 1992]. This transformation from the time domain to the frequency domain is called *Fourier transformation* based on

equation

$$H(f) = \int_{-\infty}^{\infty} h(t) e^{2\pi i f t} dt. \tag{6.1}$$

For our classification of the oscillations, the Maximum Entropy Method (MEM), described by *Press et al.* [1992], was used. The MEM transforms the frequency f to the unit circle of the complex z-plane with the relation

$$z \equiv e^{2\pi i f \Delta}, \tag{6.2}$$

where Δ stands for the sampling interval in the time domain, also called the sample rate. With this notation, the normalized power spectrum can be written in a general form as

$$P(f) = \left| \sum_{k=-\infty}^{\infty} c_k z^k \right|^2, \tag{6.3}$$

where $c_k \equiv c(t_k)$ is the real sample function for a N-point sample with $k = 0, 1, ..., N-1$.

Based on equation (6.3) a rational function for the MEM is derived, namely,

$$P(f) \approx \frac{1}{\left| \sum_{k=-M/2}^{M/2} b_k z^k \right|^2} = \frac{a_0}{\left| 1 + \sum_{k=1}^{M} a_k z^k \right|^2}. \tag{6.4}$$

By calculating the MEM, an auto-regressive process of the order of M is fitted to the time series of the data. The coefficients a_0 and a_k with k = 0, 1, ... M represent linear prediction coefficients.

The main differences between the approximation of (6.3) and equation (6.4) is that the latter can have poles on the unit z-circle. Real frequencies in the Nyquist interval can be represented with the MEM where a simple FFT can only represent zeros and not poles at real frequencies in the Nyquist interval [*Press et al.*, 1992].

For our analysis, the number of auto-regressive processes (M) was chosen to be 40 with $k = 5000$ sampling points. The significance level was set to 97% in a Chi-square distribution. To classify the runs to one of the four main oscillation patterns shown in Fig. 6.1, only the time of freshwater perturbation was considered, where the first 200 years after the start of the perturbation were not taken into account. The variance in the time series from year 200 to 1,000 was then analyzed with the MEM as described above.

Based on MEM, all performed runs were classified as followed:

- Runs with a significant power below 80 years (frequency $<$ 0.08 [1/year]) and an overturning circulation in the "on" state after the perturbation were classified as *No Oscillation*. The significance in the low-frequency spectrum is due to the variability in the MOC, which occurs in every simulation.
- Runs with a significant power larger than 200 years (frequency $>$ 0.2 [1/year]) and an overturning circulation in the "on" state after the perturbation were classified as *Oscillation Type 1*.

- Runs with a significant power larger than 200 years (frequency > 0.2 [1/year]) but an overturning circulation in the "off" state after the perturbation were classified as *Oscillation Type 2*.
- Runs with a significant power below 80 years (frequency < 0.08 [1/year]) and an overturning circulation in the "off" state after the perturbation were classified as $Weak\ MOC$.

The classified runs of all experiments of the sensitivity study with the four world settings are summarized in Fig. 6.2. In the four sets of experiments displayed in the left column, the wind stress scaling factor was kept constant at 2 for all simulations, while the Atlantic to Pacific correction (y-axis) and the freshwater perturbation (x-axis) were gradually increased. The right column displays the four sensitivity studies where the Atlantic-to-Pacific correction was kept constant at 0.15 Sv and the other two parameters were increased. Each run is represented by a colored box. Runs classified as *No Oscillation* are shown in gray. The colors of the colorbar represent all runs classified as *Oscillation Type 1*, where the different colors quantify the variance of the amplitude of the oscillations. Runs with classified as *Oscillation Type 2* are represented by yellow and green boxes indicate experiments classified as *Weak MOC*.

Interestingly, in the "world BS closed", all runs were either classified as $No\ Oscillations$ or $Weak\ MOC$, however no oscillations were found in any freshwater perturbation experiment. Also, the amount of freshwater which is needed to lead to a shut down of the MOC is higher when the "world BS closed" is used. In the other six sets of experiments, a linear relation between the amount of freshwater applied and the Atlantic to Pacific correction or the wind stress scaling, respectively, is found. When a certain threshold of freshwater is reached, the MOC starts to oscillate, where the amplitude of the oscillations increases as the amount of freshwater is increased. When the amplitude of the oscillations is high and an upper threshold of freshwater is reached, the MOC shuts down to the intermediate level where the runs are classified as $Weak\ MOC$. Low Atlantic-to-Pacific correction fluxes and low wind stress scaling factors both lead to a reduction of the freshwater threshold which is needed to lead to oscillations in the MOC. Interestingly, runs classified as *Oscillation Type 2* can mostly be seen for the "world all closed". However, no well defined region of appearance of *Oscillation Type 2* is found. They occur randomly when the freshwater perturbation is already quite high and when other runs with a similar parameter setting are classified as $Weak\ MOC$.

The similar distribution of the oscillations in the sensitivity study of the "new world", "world IP closed" and "world all closed" lead to the assumption that all oscillations have a common physical or numerical driving factor which causes the Atlantic MOC to oscillate. However, this mechanism does not work in the experiments with the "world BS closed". Something seems to be different in this setup, preventing the oscillations in the Atlantic MOC to occur. It is important to identify the mechanism which lead to oscillations in the MOC and to distinguish the reason which leads to a stable MOC in the "world BS closed". In the coming sections, the different states of the Atlantic MOC during oscillations is characterized and links are made to factors which might be a trigger for the appearance of oscillations in the MOC.

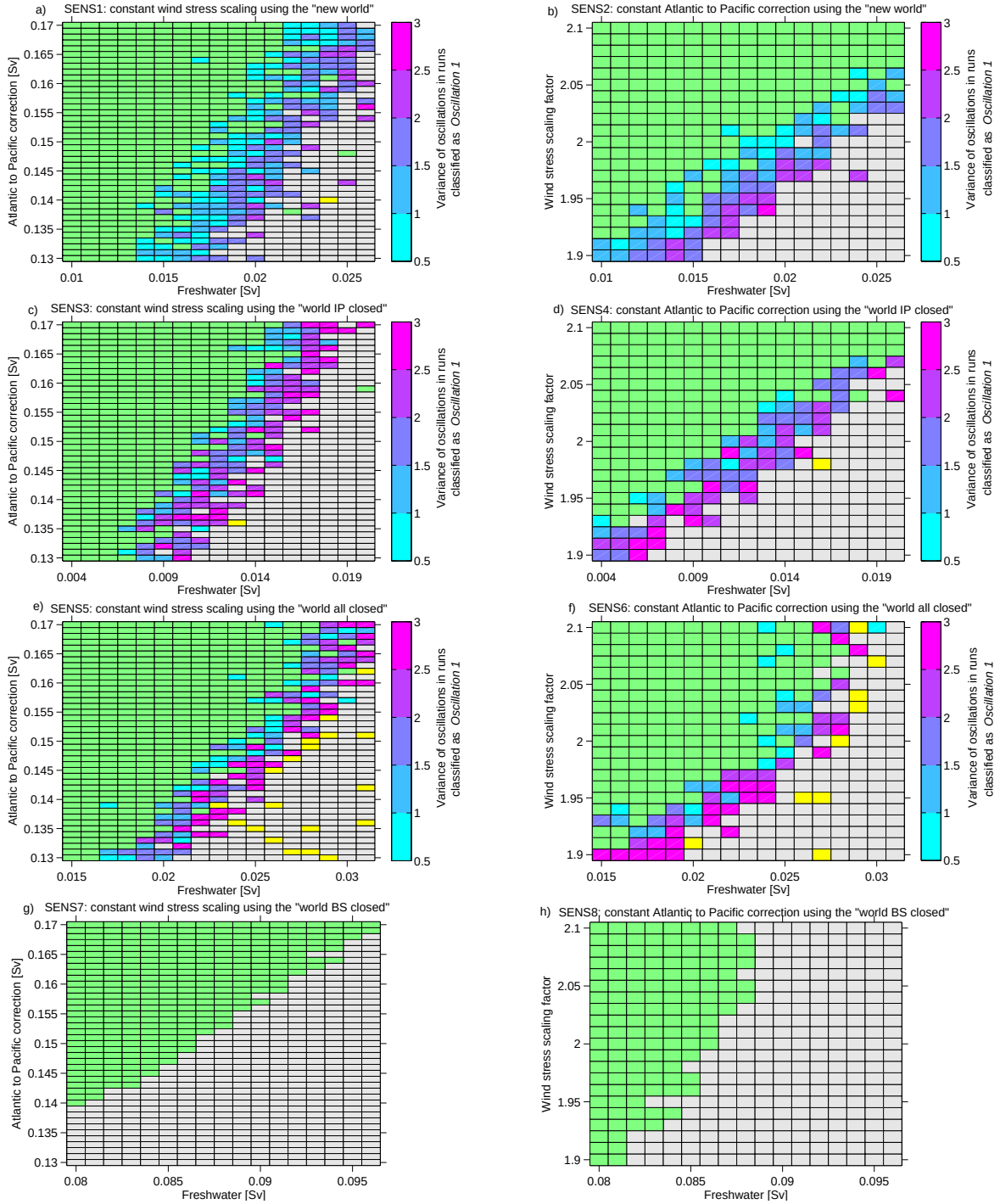

Figure 6.2: Classification of the oscillations in freshwater experiments when either the Atlantic to Pacific freshwater correction or (y-axis, left column) or the wind stress scaling factor (y-axis, right column) are changed. The strength of the freshwater perturbation is displayed on the x-axis. Boxes colored in green (■) indicate runs classified as *No Oscillation*. Runs classified as *Oscillation Type 1* are represented by the colors in the colorbar, they quantify the variance of the oscillations. Runs classified as *Oscillation Type 2* are represented by yellow (■) and gray boxes (■) indicate runs classified as *Weak MOC*.

6.3 Characteristics of the Oscillations

This section discusses the characteristics of the oscillations. For this purpose, the run displayed in Fig. 6.1b) is analyzed at in detail. Henceforth, this run is called OCHAR, the parameter setup for the run can be found in Tab. 6.2. The part of the simulation which is dominated by the oscillation is shown in Fig. 6.3; the red circles indicate the sequences in the oscillation which will be discussed in detail in this section. The sequence before the start of the perturbation at the year 0 is called stage **A**, the time when the MOC is in the first minimum is denoted stage **B** and stage **C** is when the MOC is in the first maximum.

Name of experiment	OCHAR
amount of freshwater	0.014 Sv
duration of perturbation	1,000 years
shape of freshwater pulse	rectangular
name of world setting	"world IP closed"

Table 6.2: Parameter setup for the run OCHAR.

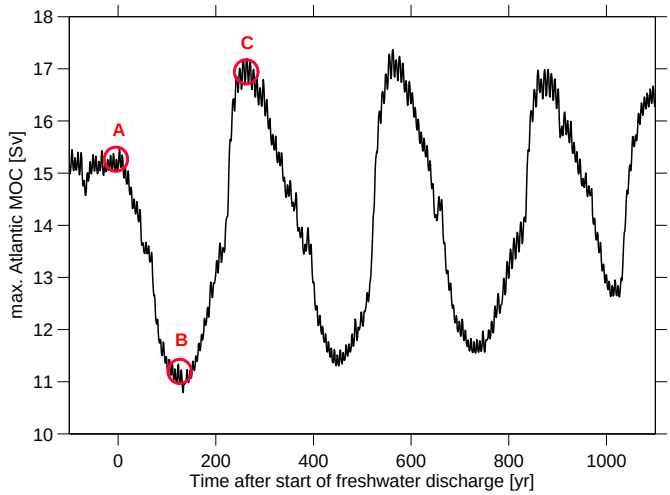

Figure 6.3: Time series of the part of the simulation (see Tab. 6.2) which is dominated by the oscillations. The red circles indicate the periods of the time series, where the convection, salinity and the barotropic stream function are analyzed. Note that the time series is smoothed by a 5-year running mean filter.

6.3.1 Salinity and Convection

Two sets of salinity profiles for the three stages **A** to **C** are shown in Fig. 6.5. The profiles a-c are based on the blue path in Fig. 6.4, while the profiles d-f correspond to the red path. When the MOC is in stage **B**, the North Atlantic in both profiles (Fig. 6.5b and e) is fresher than before the start of the perturbation (Fig. 6.5a and d). Interestingly, this freshening is not only restricted to the surface of the ocean, but also in depth below 1,000 m south of Greenland, where a fresh tongue the south can be observed. In the GIN Sea at 71°N, the whole column

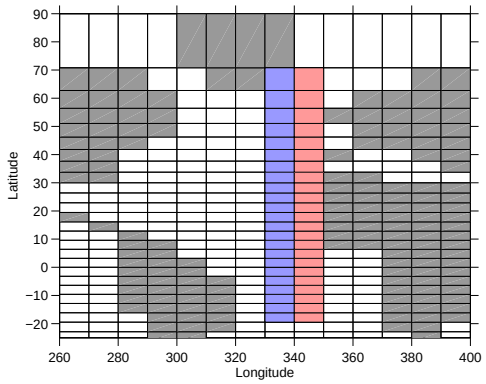

Figure 6.4: Path for the salinity profiles in Fig. 6.5: blue for the Figs. a-c and red for the Figs. d-f.

is approximately 0.5 psu fresher when the MOC is in a minimum (Fig. 6.5b) compared to the state before the perturbation (Fig. 6.5a). An even stronger freshening can be seen in the profile more to the east at the same latitude, where the freshening is most pronounced in the top 50 m (Fig. 6.5e). This leads to a stratification in this box, which prohibits deep water formation. Therefore the freshening at this latitude is highly responsible for the slowdown of the overturning circulation. When the MOC is in stage **C** (Fig. 6.5c and f), the Atlantic is overall saltier at all depths.

The changes of SSS and shuffling convection between the three stages give a more detailed view on the characteristics of the oscillation (Fig. 6.6). The two Figs. at the top display the SSS (Fig. 6.6a) and convection (Fig. 6.6d) values before the perturbation in stage **A**. The differences in stage **B** and **C** with respect to the initial values of stage **A** are shown in Fig. 6.6b-c for SSS and in Fig. 6.6e-f for convection.

The boxes of deep water formation in the GIN Sea are significantly fresher when the Atlantic MOC is at a minimum (Fig. 6.6b), especially the box more to the east displays salinity anomalies of almost 1 psu. This corresponds to the significant decrease in the shuffling convection in this region (Fig. 6.6e). The convection in the column more to the east (at 15°W) stops completely, while the box closer to Greenland still has a reduced shuffling convection and prevents the MOC to shutdown completely. The stronger convection at the west coast of Europe does not have an impact on the circulation, since convection only occurs in the topmost layers and therefore does not have an impact on the formation of deep water. When the MOC is in stage **C**, the SSS in the GIN Sea (Fig. 6.6c) is slightly higher than before the perturbation. Also the convection has increased its strength in the column at 15°W, which leads to the enhanced Atlantic MOC.

In Fig. 6.6b and c, quite strong fluctuations in the SSS anomalies in the Atlantic between 35°N and 55°N can be observed. When the MOC is in stage **B**, the Atlantic around 50°N is rather saline while a region of fresh water is found around 40°N (Fig. 6.6b). In stage **C**, only strongly positive SSS of one psu are located between 45°N and 60°N, but no negative SSS anomalies are found (Fig. 6.6c). These rapid changes in surface salinity occurred non linearly also during other phases, which are not shown here. In order to explain this odd pattern in

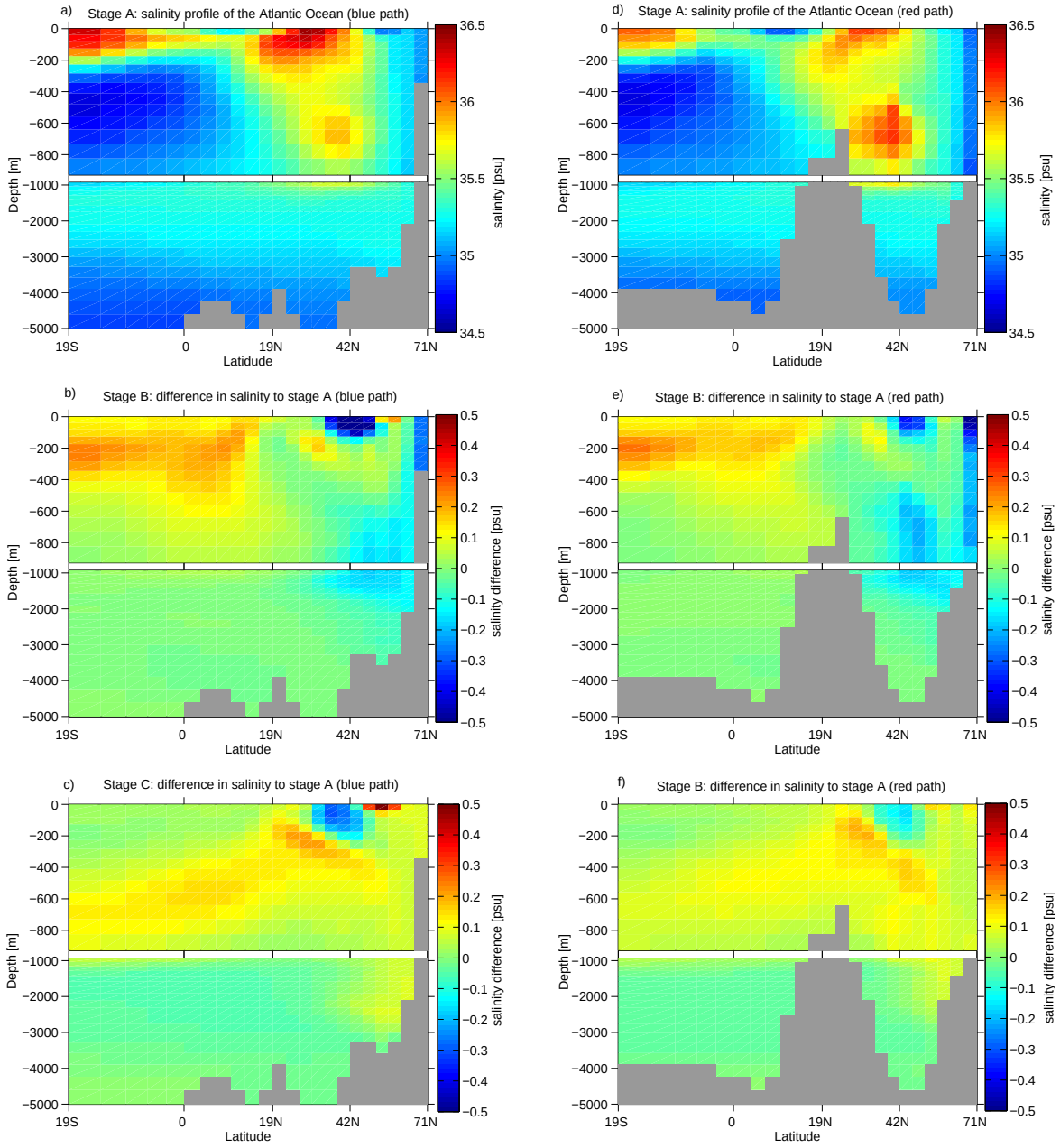

Figure 6.5: Annual mean salinity profile at three stages during a freshwater perturbation. a) to c) indicate the blue path of Fig. 6.4, while d) to f) show the red path of Fig. 6.4. Salinity before the perturbation is shown in the first row, the difference in salinity of stage **B** to stage **B** is shown in the second row. The third row shows the difference in salinity between stage **C** and stage **A**.

SSS it is necessary to have a closer look at the evolution of salinity in the North Atlantic during the freshwater discharge.

Fig. 6.7 displays a time series mean of the SSS between 45-60°N. The values represent annual mean SSS, averaged over the whole section of the North Atlantic. The chronology of the SSS (black) displays large fluctuations of approximately 0.8 psu for the whole period of time. Since

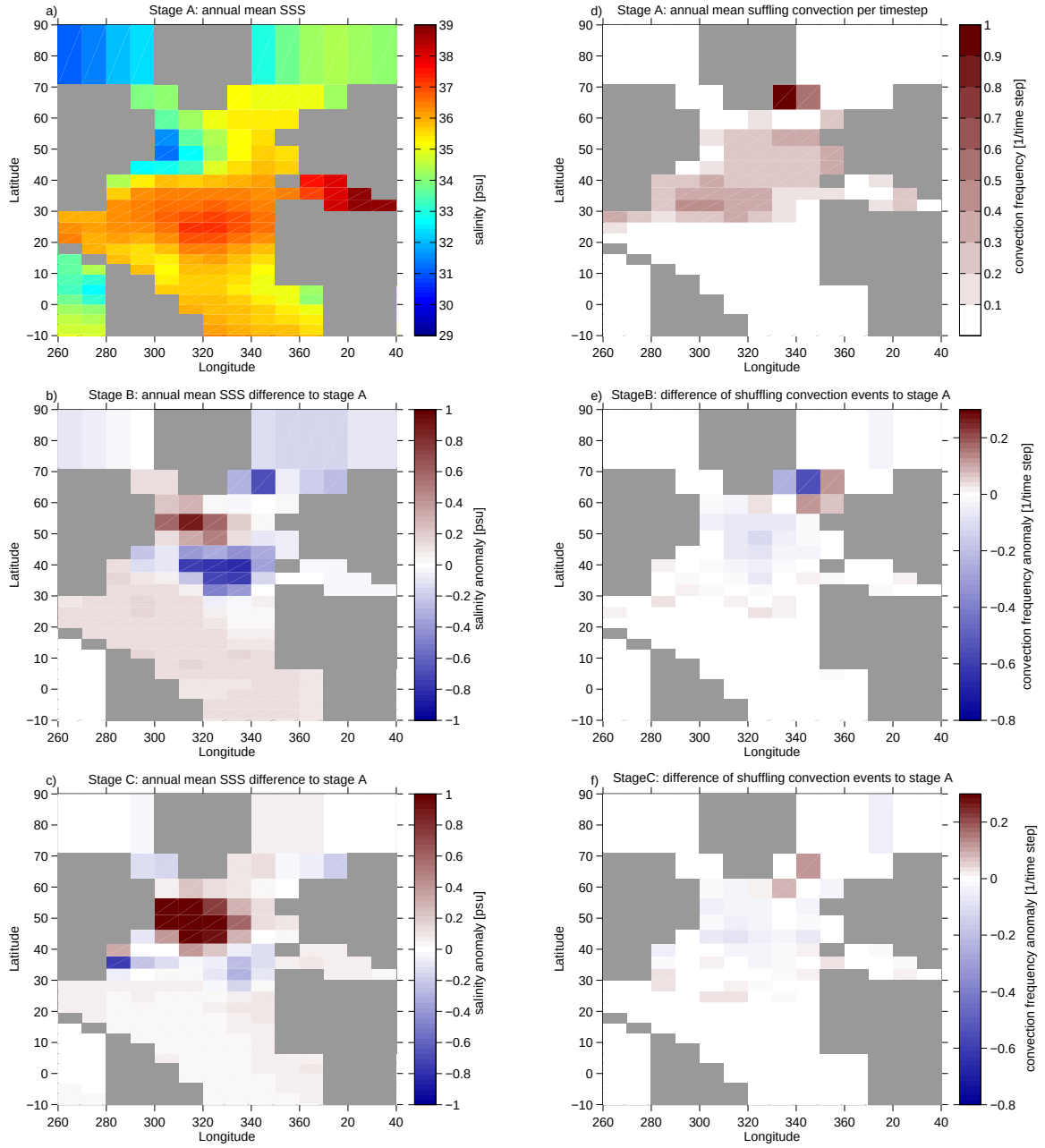

Figure 6.6: Annual mean SSS (a-c) and shuffling convection event per time step (d-e) for the three stages of the MOC. The first row shows the SSS and convection before the perturbation. The second row shows the differences of SSS and convection when the MOC is in a minimum (stage **B**) with respect to the values before the perturbation. The third row shows the differences between SSS and convection when the MOC is in a maximum (stage **C**) with respect to the values before the perturbation.

the irregularity already occurred before the start of the perturbation, they are not triggered by the oscillations of the MOC. In order to remove the noise in the time series, a 20-year running mean filter was applied (red in Fig. 6.7). A zoom on the filtered North Atlantic SSS during the 1,000 years of the freshwater perturbation is displayed in Fig. 6.8 (bottom). As

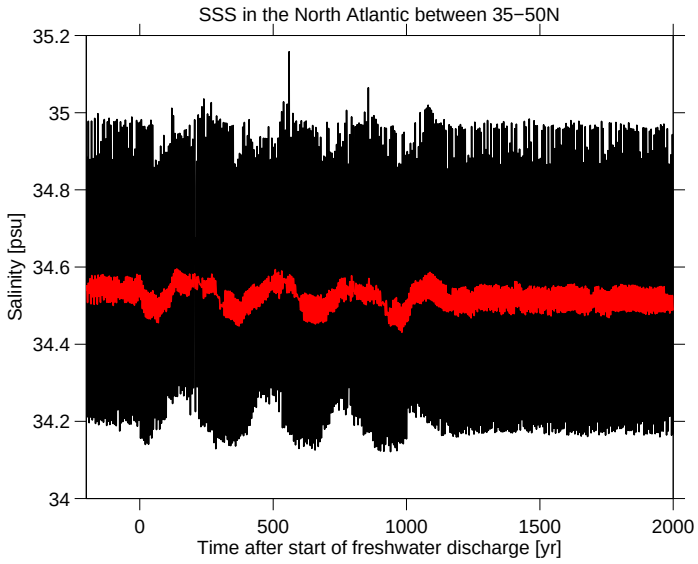

Figure 6.7: SSS in the North Atlantic between 35°N and 50°N during a 1,000 year freshwater perturbation of 0.014 Sv with the "world IP closed". The red line represents the filtered SSS values when a 20-year running mean was applied.

a reference, the Atlantic MOC is also shown (top). In the time series of salinity, oscillations can clearly be seen, however, the two time series do not evolve synchronously. Even before the MOC has reached the first minimum, the SSS already starts to increase again. When the MOC recovers from the minimum, the SSS values decrease again. The phase lag between MOC and salinity is determined by a cross-correlation between the two time series during the 1,000 years of the freshwater perturbation (Fig. 6.9). The maximum positive correlation is somewhat higher than 0.5. The Atlantic SSS leads the MOC by about 80 years.

Another interesting feature of the SSS patterns in Fig. 6.6 is that the salinities in the GIN Sea and in the Labrador Sea react opposite to each other during the oscillations. When the MOC is in stage **B**, the Labrador Sea is slightly more saline and the GIN Sea is significantly fresher than before the freshwater perturbation (Fig. 6.6b). In contrast to this, the GIN Sea is saltier in stage **C** while the Labrador Sea is fresher compared to SSS values of stage **A** (Fig. 6.6c). When looking at the time series of SSS only in these two basins (Fig. 6.10), this linkage can be nicely observed. When the freshwater perturbation starts at year 0, the SSS in the GIN Sea starts to decrease due to the slowdown of the MOC. At the same time, the Labrador Sea accumulates salt at the surface. When the MOC increases again at year 150, also the SSS in the GIN Sea start to increase while it decreases in the Labrador Sea. It is difficult to make robust statements about the origin of this anti-cyclic salinity pattern. The GIN Sea and the Labrador Sea are coarsely resolved in our model by only two boxes and therefore the dynamics within these parts of the ocean are poorly represented. However, it is likely that the salt anomaly in the Labrador Sea is linked to the overall SSS evolution in the North Atlantic basin which was shown in Fig. 6.8. The GIN Sea becomes fresher as the MOC decreases because the perturbed freshwater accumulates due to the weak convection in these two columns.

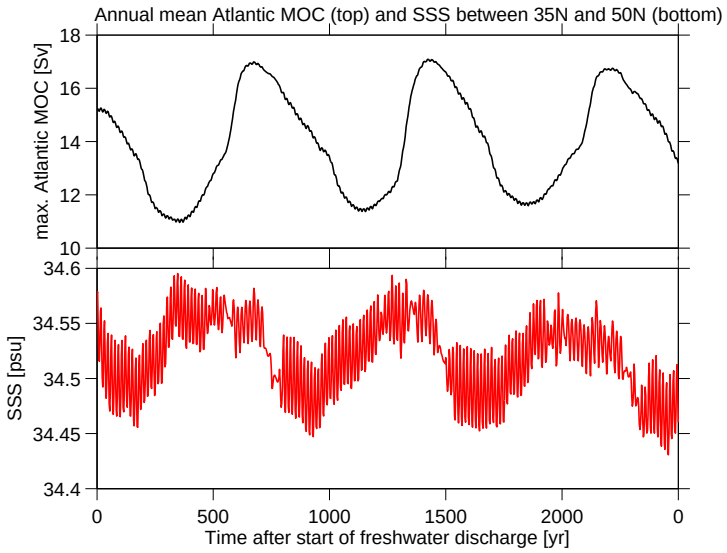

Figure 6.8: Annual mean Atlantic MOC during a 1,000 year freshwater perturbation of 0.014 Sv (top) and the corresponding SSS in the North Atlantic between 35-50°N (bottom). The two time series were smoothed by a 20-year running mean.

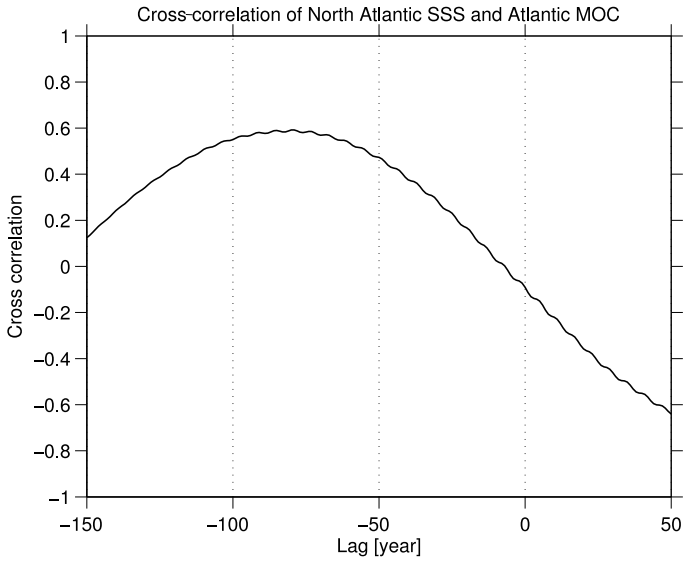

Figure 6.9: Cross-correlation between the smoothed time series of the North Atlantic SSS and the Atlantic MOC. The maximum of the positive correlation is at a lag of approximately –80 years, which indicates that the SSS anomalies precede the MOC by 80 years.

Also for the time series of the SSS in the GIN Sea and the Labrador Sea, a cross-correlation was calculated with the Atlantic MOC in order to distinguish a lead or lag of the SSS towards the MOC. Fig. 6.11 contains the two cross-correlations. A highly positive correlation of almost 1 can be seen between the SSS in the GIN Sea and the MOC (Fig. 6.11a). However,

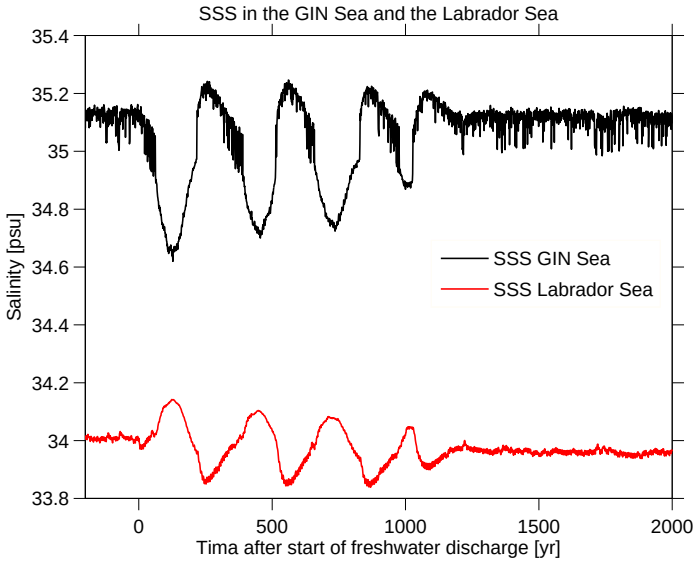

Figure 6.10: SSS in the GIN Sea (black) and the Labrador Sea (red) during a 1,000 year freshwater perturbation of 0.014 Sv. The time series were smoothed with a 10-year running mean.

the maximum of the correlation is at a lag of approximately –2 years, which means that the SSS precedes the overturning circulation by two years. A strong negative correlation can be seen for the SSS in the Labrador Sea and the MOC (Fig. 6.11b). The highest negative correlation is at a lag of approximately –5 years, indicating a lead of the SSS in the Labrador Sea to the MOC of 5 years.

In summary, a slowdown of the Atlantic MOC is linked to a decrease in convection in the GIN Sea. When the MOC is in a minimum, the GIN Sea is fresher, while the Labrador Sea and the Atlantic south of 30°N are rather salty. These positive SSS anomalies could be explained

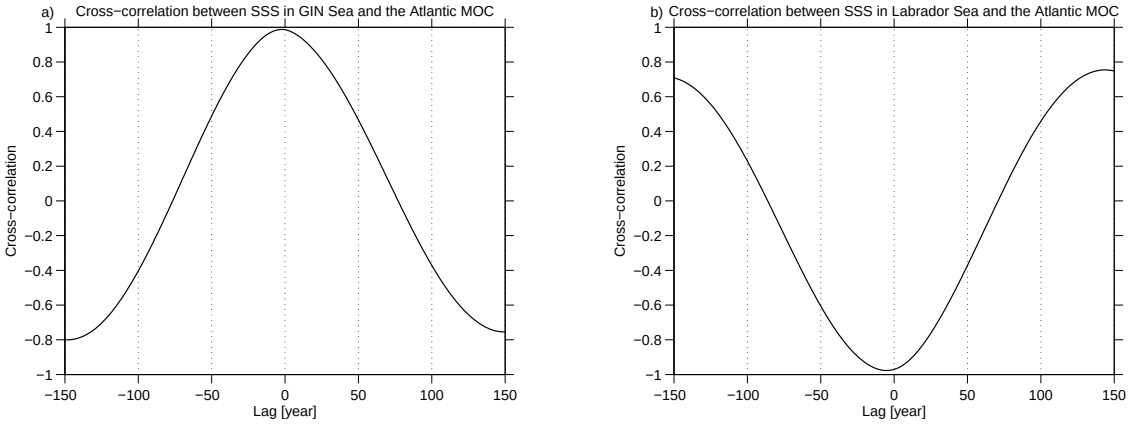

Figure 6.11: a) Cross-correlation between the smoothed time series of SSS in the GIN Sea and the Atlantic MOC. The maximum of the positive correlation at a lag of –2 years indicates a lead of the SSS to the MOC by this many years. b) Cross-correlation between SSS in the Labrador Sea and the Atlantic MOC. The maximum negative correlation is at a lag of –5 years, indicating that the SSS precedes the MOC by 5 years.

by a reduced transport of water to the high latitudes and therefore to an accumulation of surface salinity in the Atlantic Ocean. The overturning does not shut down completely and convection still takes place in one column in the GIN Sea. With this, surface salinity is still transported towards the deep water formation regions. When a threshold is reached and the SSS is high enough in the GIN Sea, it creates an unstable water column and triggers the convection to operate again. The MOC increases in strength and the salinity is flushed down. The positive salinity anomalies in the south Atlantic diminish and the Labrador Sea becomes fresher.

6.3.2 The Subpolar Gyre

The Subpolar Gyre (SPG) plays an important role in the transport of saline surface water to the region of deep water formation in the GIN Sea. Strong temporal variations in the SPG volume transport on multiple time-scales have been found in observations as well as model simulations [*Hátún et al.*, 2005; *Häkkinen and Rhines*, 2004; *Häkkinen and Rhines*, 2009]. In several studies, small present-day variations in the strength of the MOC are explained by the changes in the strength of the SPG [*Böning et al.*, 2006; *Hátún et al.*, 2005]. While the strength of the gyre is mostly wind driven [*Böning et al.*, 2006], i.e., strong wind stress enhances the strength of the gyre, also a number of internal and external mechanisms are believed to be responsible for variations in the SPG. In freshwater perturbation experiments in the North Atlantic with a coarse-resolution climate model, *Levermann and Born* [2007] found a positive baroclinic feedback within the SPG which reinforces the gyre circulation. It was shown that a strong gyre transports more tropical saline water into the subpolar region south of Greenland. This water recirculates in the gyre and increases the density in its center. The resulting gradient of salinity and density between the gyre center and the exterior leads to an even stronger gyre circulation enhancing this process. A similar positive feedback mechanism was also found for the temperature gradient between the gyre center and the surrounding ocean. In a recent study, *Born and Levermann* [2010] analyzed the freshwater outburst from the American proglacial lakes during the 8.2 K event on the strength of the Atlantic MOC. It was shown that the positive feedback mechanism withing the SPG [*Levermann and Born*, 2007] can have an effect on the stability of the Atlantic MOC during freshwater perturbations.

Based on this theoretical background, the SPG is analyzed in detail in this section. It is clear that due to the coarse resolution of our model, the dynamics of the SPG are only weakly represented and do not exhibit the observed excursions in the Labrador Sea and the in GIN Sea. Also the strength of the circulation is underestimated. Because of this, the small-scale internal feedbacks suggested by *Levermann and Born* [2007] cannot be reproduced in the same way in our model. However, this section still tries to give an overview on the dynamics of the surface circulation in the North Atlantic. The goal is to get a better understanding of the oscillations and to find a possible link between the gyre strength and the overturning circulation.

Fig. 6.12 shows the barotropic streamfunction in the North Atlantic for the three stages **A** to **C** of the oscillation. The circulation consists of two gyres, namely the Subpolar gyre (SPG) and the Subtropical gyre (STG). The strength of the STG does not respond much to the oscillations and is nearly constant. The SPG decreases significantly in strength by about 7 Sv when the MOC is in a minimum compared to the circulation before the perturbation. When

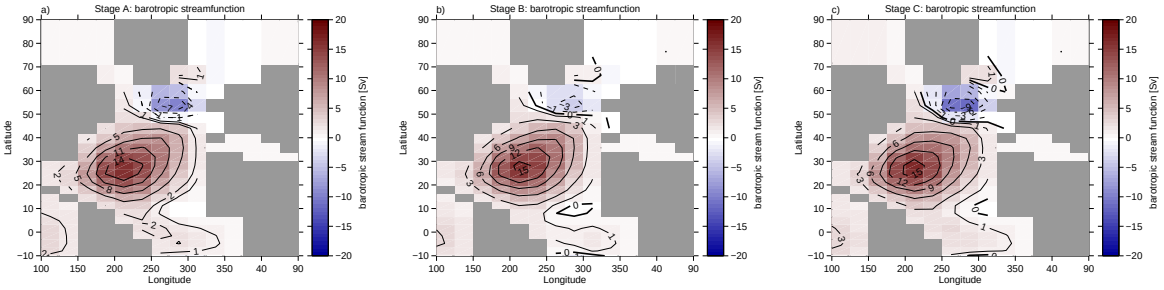

Figure 6.12: The barotropic streamfunction in the North Atlantic a) before the perturbation (stage **A**), b) in a minimum of the MOC (stage **B**) and c) in a maximum of the MOC (stage **C**). Positive values indicate a clockwise circulation, negative values stand for an anticlockwise circulation.

the Atlantic MOC is in stage **C**, the circulation of the SPG is approximately 2 Sv stronger than it was before the perturbation. The strength of the Subtropical Gyre (STG) does not respond much to the oscillations and is nearly constant.

In order to understand the development of the SPG during the oscillations, the maximum strength of the SPG for the whole duration of the perturbation is shown in Fig. 6.13. When the MOC decreases in strength at the start of the freshwater perturbation, also the SPG immediately slows down and synchronously oscillates with the MOC for the whole duration of the perturbation. When comparing the two time series in Fig. 6.13, a slight lead of the SPG with respect to the MOC can be observed. The calculation of a cross-correlation between the two values allows a quantification of their relationship (Fig. 6.14). The maximum of the positive correlation can be seen at a lag of –7 years, which indicates a lead of the SPG towards the Atlantic MOC by 7 years.

The interpretation of the results from the cross-correlation is difficult as the SPG in our model is only represented by 8 boxes. The stabilizing effect of the gyre, due to internal

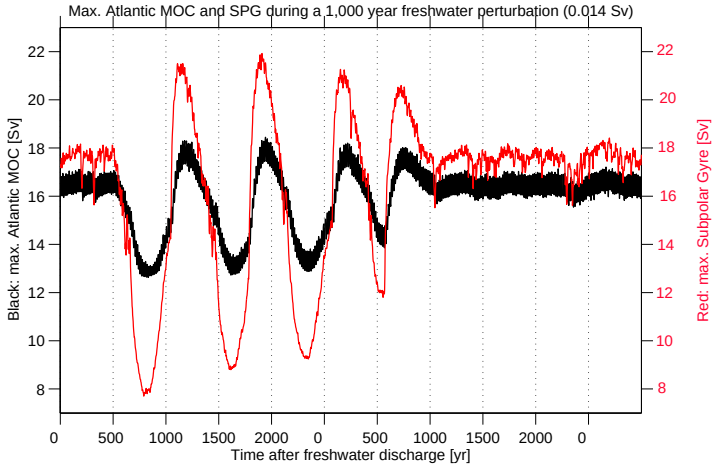

Figure 6.13: Annual mean Atlantic MOC [Sv] (black) and maximum strength of Subpolar Gyre [Sv] (red) during a freshwater perturbation of 0.014 Sv with the "world IP closed".

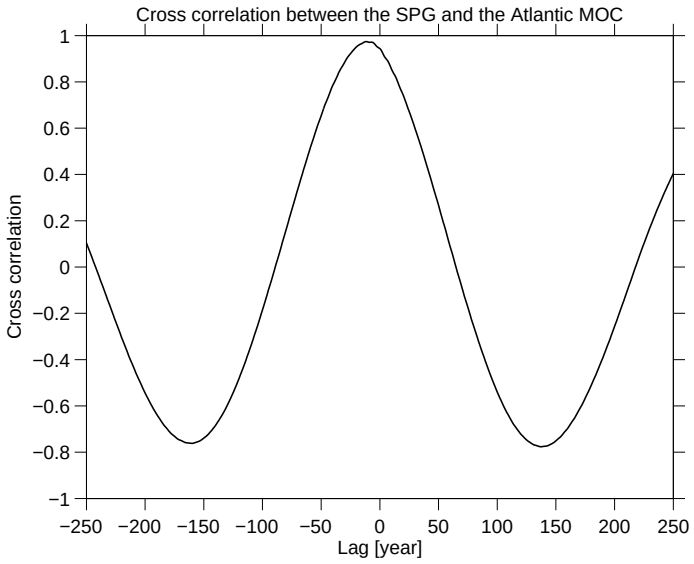

Figure 6.14: Cross-correlation between strength of the Subpolar Gyre and the maximum Atlantic MOC (both instantaneous values at the beginning of the year). The maximum correlation is at a lag of approximately –7 years, indicating that the SPG precedes the MOC by this amount of time.

salinity and temperature feedbacks, could not be reproduced in our model, mainly because of the numerical instabilities of SSS in the subpolar region (see section 6.3.1). Also the coarse resolution of the Bern3D model and the incomplete representation of dynamics in the North Atlantic do not allow robust interpretations on the effect of salinity on the gyre.

In the study by *Hátún et al.* [2005] it was shown based on observational data and high-resolution model simulations, that a decreased strength of the SPG leads to an enhanced transport of saline surface water towards the GIN Sea. In contrast to this, it was shown that a strong gyre transports less SSS towards the GIN Sea but leads to higher salinity in the subpolar region south of Greenland. Based on this study, a link between the strength of the SPG and the MOC can be established. The increased transport of water towards the region of deep water formation in the GIN Sea in a phase where the MOC is weak would also lead to a high transport of SSS towards this region. A slight increase in surface density in the GIN Sea can be enough the cause a a destabilization of the water column and lead to a recovery of the Atlantic MOC. The strength of the gyre therefore plays an important role on the resumption of the MOC.

6.3.3 Velocity of Ocean Currents

So far, only processes within the Atlantic Ocean have been studied. It has been shown that the resumption of the MOC could be linked to an increased transport of salinity to the GIN Sea. It was assumed that the water originates from the Atlantic Ocean. However, it is also possible that the oscillations are caused by changes in flow velocities between the ocean basins, and linked to this, by a shift in salinity or freshwater import into the Atlantic Ocean. *Weijer et al.* [2001] analyzed the impact of the inter-ocean fluxes of heat and salt via the Agulhas Leakage at the south tip of Africa, the Drake Passage and the Bering Strait on the

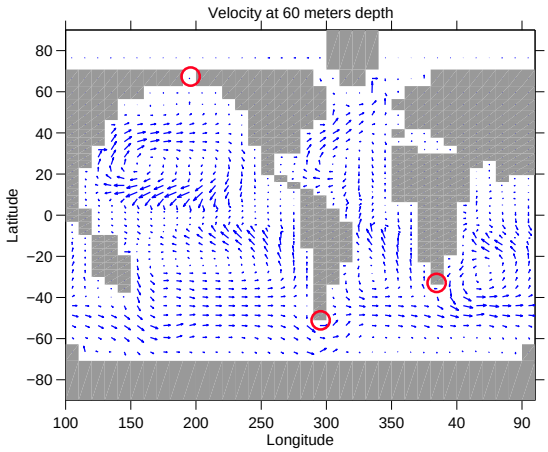

Figure 6.15: Velocity vectors at a depth of 60 meters. The red circles indicate the boxes where a time series of the velocity is shown in Fig. 6.16.

stability of the Atlantic MOC. They found a stabilizing effect on the MOC of the salinity flux in the Agulhas Leakage, while the freshwater import through the BS into the North Atlantic has a destabilizing effect on the circulation. This section analyzes the velocities of ocean currents between the ocean basins and tries to see if the oscillations are linked to alteration of inter-ocean fluxes.

In a recent study, *Biastoch et al.* [2008] suggest an influence of the dynamics in the region of the Agulhas Leakage on the variability of the MOC. It is therefore possible that a different salt flux south of Africa during the oscillations might influence the development of the overturning circulation. Also the import of water from the Pacific into the Atlantic south of South America is investigated to see if significant changes can be related to the oscillations. Finally, the flux through the BS into the Arctic Ocean and the North Atlantic is examined. A reversed flow during the oscillations would be an indicator for export of fresh water from the Atlantic into the Pacific. This could be an explanation for the restart of the MOC.

An overview on the global flow vectors at a depth of 60 meters is given in Fig. 6.15. The depth-integrated velocities in the longitudinal-direction in the three regions highlighted by a circle are shown in Fig. 6.16b-d. The Atlantic MOC is given as a reference (Fig. 6.16a). Note that all velocities are in ms^{-1} where positive values indicate an eastward flow while negative values stand for a flow towards the west. The velocities in all three regions oscillate with the MOC and decrease in strength when the MOC is weaker. Interestingly, none of the considered currents change the direction during the oscillations, which is an important finding for the interpretation of the oscillations. An export of fresh water through the BS or an export of saline water into the south Atlantic would have explained the resumption of the MOC.

The velocity of the water flux in the Agulhas Current south of Africa (Fig. 6.16c) already starts at a very low pace and decreases even more as the MOC reduces in strength. Also, no lag in time is observed between the time series of the velocity and the Atlantic MOC. Therefore, it is rather unlikely that the flow through the Agulhas Leakage in our model has a large influence on the Atlantic MOC, as it is suggested in a recent study by *Biastoch et al.*

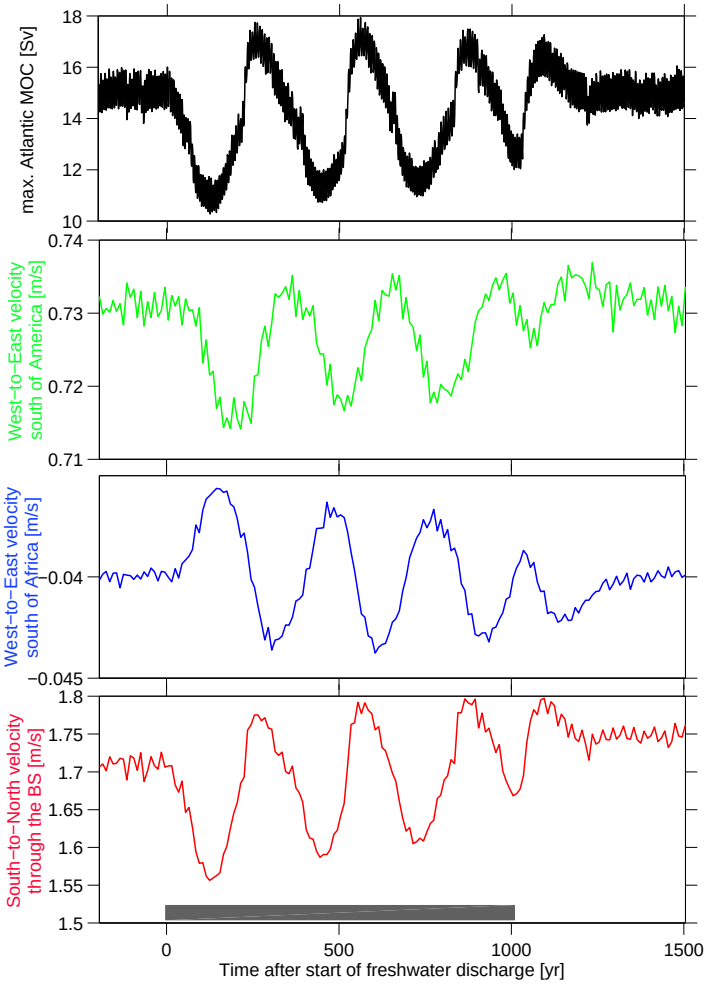

Figure 6.16: a) Atlantic MOC [Sv] and the depth-integrated velocity of ocean flow [ms^{-1}] at the three regions marked with circles in Fig. 6.15: b) flux south of South America from the Pacific into the Atlantic, c) flux from the Indian Ocean into the Atlantic at the south peak of Africa and d) flux in the Arctic Ocean which passes through the BS into the Atlantic. The gray bar indicates the duration of the freshwater perturbation.

[2008]. Since not much more salinity is imported into the south Atlantic Ocean during the oscillations, the positive SSS anomalies must originate mainly from the Atlantic Ocean itself. When observing the evolution of velocity south of America (Fig. 6.16c), also a decrease of the inflow into the Atlantic can be seen. Interestingly, the velocity only starts to decrease about 90 years after the start of the freshwater discharge. It is possible that the decreased import of fresher water from the Pacific has an effect on the positive SSS anomalies in the South Atlantic which can be observed during the period of a low Atlantic MOC (see section 6.3.1). However, since the transport of water through the whole Atlantic Ocean takes about 150 to 200 years, it is difficult to quantify these effects on the resumption of the Atlantic MOC.

Name of experiment	FV
max. positive freshwater	0.014 Sv
duration of positive perturbation	3,000 years
shape of freshwater pulse	rectangular
name of world setting used	"world IP closed"

Table 6.3: Parameter setup for the run FV. Note that the world setting and the amount of freshwater is the same as in the experiment displayed in Fig. 6.1b)

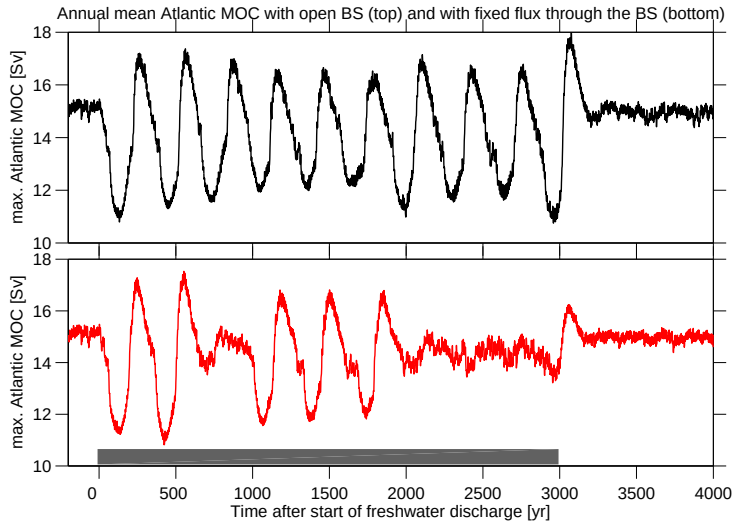

Figure 6.17: Annual mean Atlantic MOC of the experiment FV (see Tab. 6.3). Top: the velocity through the BS was not kept constant, bottom: the velocity through the BS was fixed to the value before the start of the perturbation. The time series was filtered with a 5-year running mean. The gray bar indicates the duration of the freshwater perturbation.

Also, the Drake Passage in our model is three boxes wide. The consideration of the depth-integrated flux in one column only does not allow any robust statements on the dynamical impact of the total inflow into the southern Atlantic.

When observing the flow from the Pacific through the BS into the Arctic Ocean, also a decrease of the velocity is found when the MOC is weaker, while the flux accelerates as the MOC becomes stronger (Fig. 6.16d). However, as mentioned above, there is no flux out of the Atlantic at any time, which means that the perturbed freshwater is not exported from the Atlantic into the Pacific. Interestingly, a slight trend towards higher velocities can be seen in the time series as the oscillations evolve. After the perturbation, the velocity is slightly higher than it was before the start of the discharge.

In order to identify the effect of the velocity changes from the North Pacific into the North Atlantic, the velocity through the BS was kept constant. This prevents the velocity in the Arctic Ocean to oscillate. The goal was to see if the fixed velocity has an impact on the occurrence of oscillations in the Atlantic MOC, or whether the oscillation stops. The experiment is called FV and the parameter setup is listed in Tab. 6.3. Note that the overall parameters

are the same as in the experiment OCHAR (Tab. 6.2), however the duration of the pulse was increased to 3,000 years in order to analyze the long-term development of the Atlantic MOC.

The time series of the Atlantic MOC of the experiment FV is displayed in red in Fig. 6.17. For comparison, the time series of the MOC for the same experiment without a fixed velocity through the BS is shown in black. When the BS velocity is not fixed, the MOC oscillates during the entire freshwater perturbation. Strong oscillations in the overturning circulation are also found in the experiment FV at the beginning of the perturbation for about 750 years. Then there is a transition, where the MOC seems to be stable for a short period of time, before the oscillations restart again, this time with a slightly lower amplitude. During the last 1,000 years of the perturbation only very weak oscillations are found. Based on these findings, the flow through the BS seems to have only a partial impact on the stability of the MOC. Other factors as discussed in the previous sections must play a more important role on the oscillations than the flow from the Pacific into the Atlantic Ocean.

In summary, all velocities oscillate in response to the oscillations in the Atlantic MOC. Even though the direction of the flow does not change during the oscillations, a reduced flux of salinity into the Atlantic Ocean can have an effect on convection in the North Atlantic and therefore on the strength of the MOC. A prescribed fixed velocity through the BS results in slightly damped oscillations, however a total absence of oscillations in the MOC was not found. This leads to the conclusion that the open BS is not the only driving factor causing oscillations in the Atlantic MOC.

6.3.4 The Role of the Bering Strait

Even though some parameters, e.g. accumulation of SSS in the Atlantic, were detected which might be a cause for the oscillations, it still remains unclear why no oscillations occur in the world setting "world BS closed" in any freshwater experiments, while the Atlantic MOC of the three other world setups oscillates at a certain freshwater perturbation amount (see section 6.2.1). The role of a closed BS on the stability of the Atlantic MOC is therefore analyzed in this section. For this purpose, one experiment where the "world BS closed" was used is analyzed in detail. The run is called BSC and the parameters used in this experiment are summarized in Tab. 6.4. Fig. 6.18 shows the annual mean values of the Atlantic MOC. The red circles label the four stages during the run which will be focused on, one before the start of the perturbation, two during the perturbation at years 400 and 900 and one after the end of the discharge at year 1500.

The Atlantic MOC decreases abruptly at the beginning of the perturbation to about 12.5 Sv. From there a gradual decrease of the MOC can be seen until the overturning circulation reaches a minimum strength of approximately 12 Sv at year 1,000. After the perturbation, the MOC recovers to a stronger circulation but does not reach the "on" state as before the perturbation anymore. At all times, quite strong fluctuations in the MOC can be seen, even though the time series has been filtered.

In a study by *De Boer and Nof* [2004], an important role on the stability of the Atlantic MOC is assigned to the Bering Strait. It is suggested that during an interglacial period when the BS is open, freshwater input into the North Atlantic is flushed out through the BS. However, a closed BS, e.g., during a glacial period, trapped the freshwater in the North Atlantic leading

Name of the experiment	BSC
max. positive freshwater	0.02 Sv
duration of positive perturbation	1,000 years
shape of freshwater pulse	rectangular
name of world setting used	"world BS closed"

Table 6.4: Parameter setup for the run BSC.

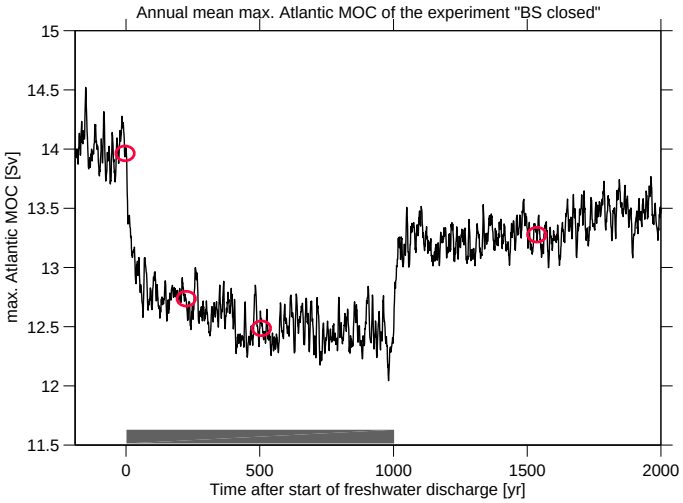

Figure 6.18: Annual mean values of the max. Atlantic MOC for the run BSC. During 1,000 years 0.02 Sv of freshwater was perturbed in the North Atlantic, the "world BS closed" setting was used for this experiment. Note that the time series was filtered with a 5-year running mean in order to remove low-frequency fluctuations in the time-series. The gray bar indicates the duration of the freshwater perturbation.

to a slowdown of the MOC.

The distribution of the SSS at different times during and after the perturbation with respect to the values before the discharge can be seen in Fig. 6.19b-d. The distribution of SSS before the perturbation at year 0 is shown as a comparison (Fig. 6.19a). They were discussed in detail in section 4.2.2. As the freshwater is perturbed, the negative SSS anomalies in the Arctic Ocean increase gradually (Fig. 6.19b and c). Especially east of Greenland, the freshwater accumulates and the anomalies are the most pronounced. Interestingly, the subpolar region south of Greenland does not become much fresher at any time during the perturbation. Also, no accumulation of SSS is found in the south Atlantic during the perturbation, which is in contrast to the MOC oscillations (see section 6.3.1). Even 500 years after the end of the perturbation, the Arctic Ocean is rather fresh (Fig. 6.19d). This findings support the hypothesis of *De Boer and Nof* [2004], who suggest a trapping of freshwater when the BS is closed.

The question still remains though why oscillations occur in the "world all closed" while no oscillations can be observed when only the BS is closed. An answer to this is found in the pattern of convection. Fig. 6.20a displays the shuffling convection events per time step before

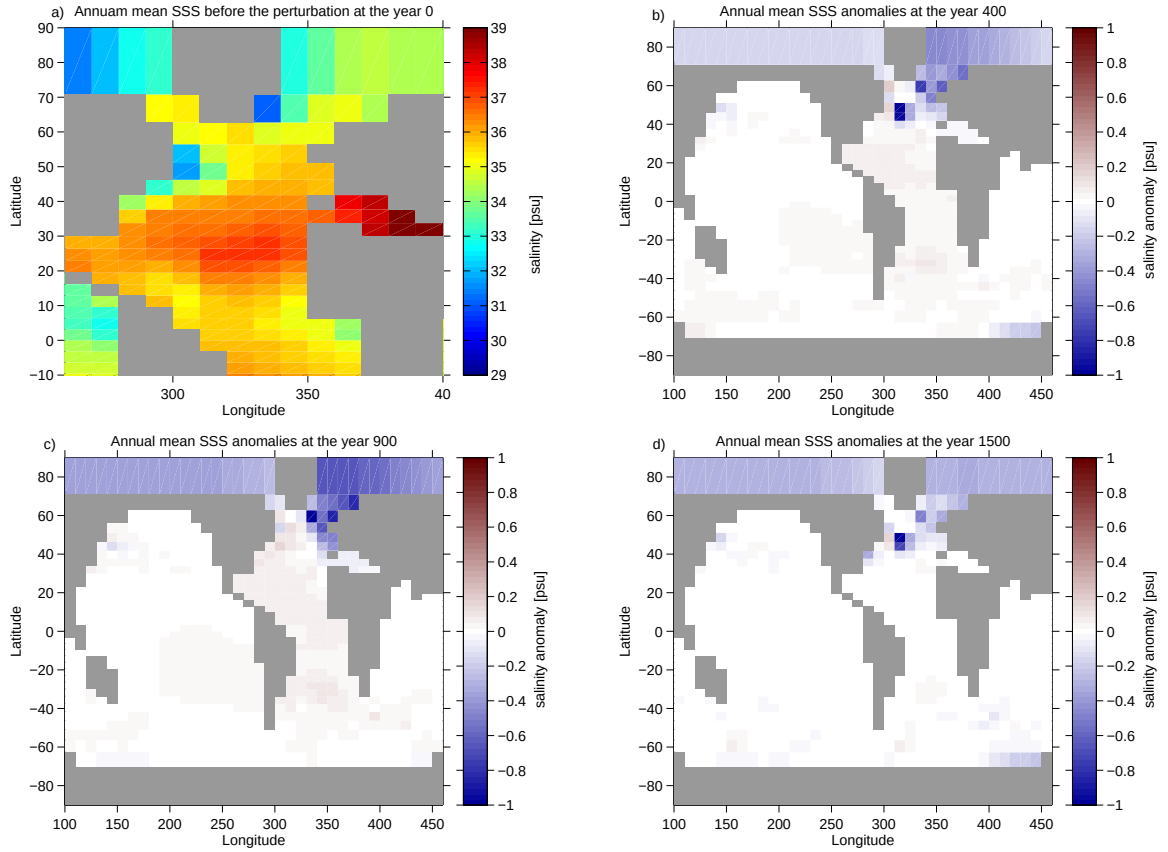

Figure 6.19: a) Annual mean values of SSS in the North Atlantic and the anomalies in SSS during the perturbation at the year b) 400 c) 900 and d) 1500 with respect to the values before the perturbation at the year 0 for the experiment BSC. These time points are indicated in Fig. 6.18.

the perturbation, the differences in convection at years 400, 900 and 1500 with respect to the convection frequency before the perturbation is shown in the Fig. 6.20b-d. Even before the perturbation starts (Fig. 6.20a), convection is most pronounced south of Greenland, but no deep water formation takes place in the GIN Sea. This pattern is very different to the convection before the perturbation of the run OCHAR (Fig. 6.6d), where mainly in the GIN Sea strong shuffling convection is observed. During the perturbation, the convection decreases only very slightly south of Greenland.

The convection of the run BSC takes place in the same water column south of Greenland as in the steady "intermediate" state (see section 5.2). This seems to stabilize the MOC and leads to a more stable state of the model than when convection takes place only in the GIN Sea.

In summary, the open BS does not directly affect the occurrence of oscillations in the MOC. More important is the steady state of the model before the perturbation and the location of deep water formation. Apparently, strong convection south of Greenland is more stable than convection in the GIN Sea only.

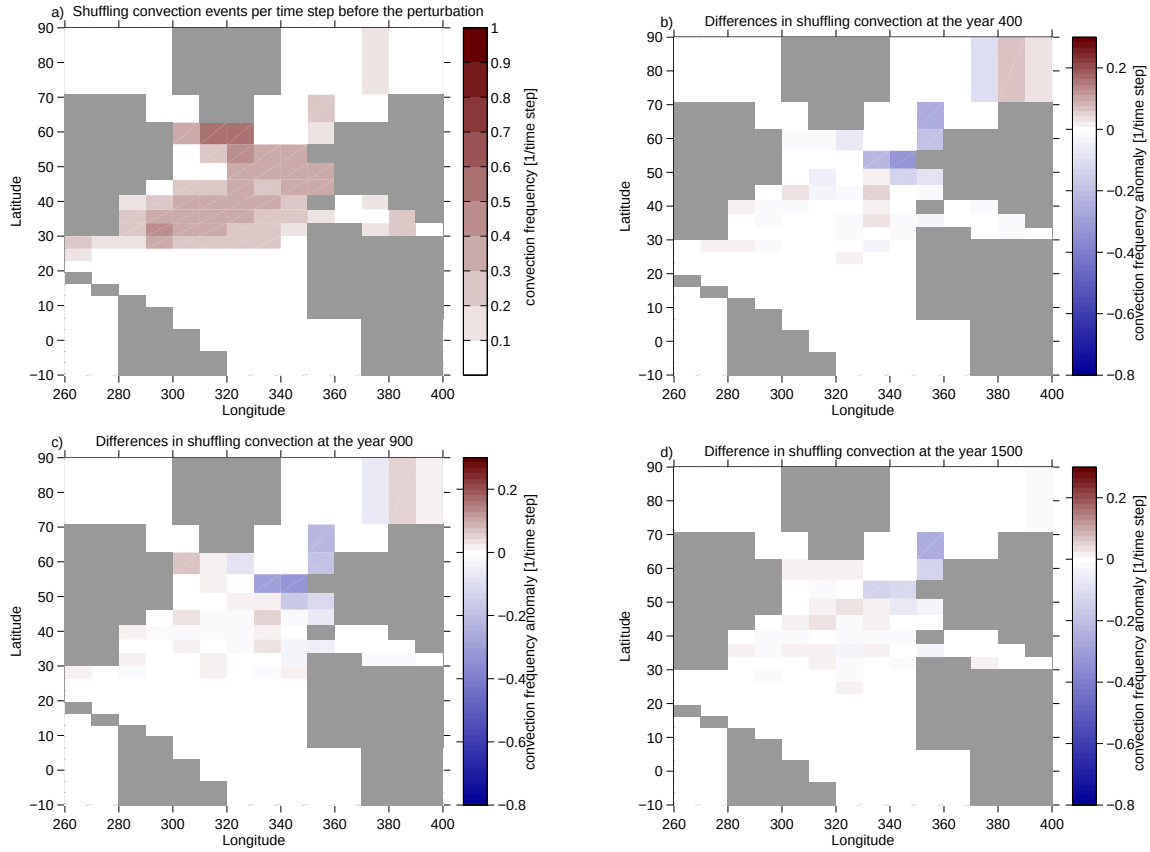

Figure 6.20: Differences in annual mean shuffling convection frequency during the perturbation at the year a) 400 b) 900 and c) 1500 with respect to the values before the perturbation for the experiment BSC.

6.3.5 Summary

In a number of freshwater forcing experiments in the North Atlantic, oscillations were detected in the Atlantic MOC when the model was run with the "new world", the "world IP closed" or the "world all closed" setting. In all the experiments, the range for the amount of freshwater to cause oscillations is very narrow and lies between 0.004 to 0.031 Sv. When the amount of freshwater is too small, no oscillations occur and after a certain upper threshold, the MOC shuts down to a lower but stable circulation. No oscillations appeared in the experiments performed with the "world BS closed". In this world setup, a higher amount of freshwater of 0.08 to 0.96 Sv needs to be applied in order to shut down the Atlantic MOC. The Atlantic to Pacific freshwater correction and the wind stress scaling do not have an impact on the occurrence of oscillations. However, by increasing one of these two parameters, the threshold of the amount of freshwater which is needed to cause oscillations is higher.

The existence of oscillations can be related to an interplay of two negative physical feedback mechanisms, causing the MOC to fluctuate between a strong and a weak stage. It is driven by the SSS anomalies in the southern Atlantic and the strength of the SPG. A weak MOC leads to a decreased transport of surface salinity towards the high latitudes and therefore to an accumulation of positive SSS anomalies below 45°N. On the other hand, a weak overturning circulation decreases the strength of the SPG, which in turn increases the transport from the

subtropics to the GIN Sea [*Hátún et al.*, 2005]. The highly saline water is transported towards the deep water formation region in the GIN Sea and causes an instability in the water column. The convection in the GIN Sea restarts and leads to an increase in the Atlantic MOC. Positive SSS anomalies which have accumulated in the southern Atlantic Ocean are flushed and the feedback loop restarts again. A schematical illustration of this stabilizing negative feedback mechanism is shown in Fig. 6.21. The signs attached to the arrows indicate the correlation between changes in the quantities of the two linked boxes. The circled signs in the centers of the two loops represent the resulting correlations. Because of the two negative feedbacks loops, processes are damped, and this leads to a self-stabilizing mechanism in the system.

Besides, the abrupt shutdown of the MOC after a sequence of oscillations (see Fig. 6.1c) can be explained with this feedback mechanism. The oscillations are also triggered by positive SSS anomalies which are transported to the GIN Sea. However, when the SSS anomalies in the region around 45°N are not high enough, the MOC can not recover anymore and stays at the low level for the rest of the perturbation (Fig. 6.22). It still remains unclear though why the SSS anomalies vanish suddenly. The question about the reason why the abrupt slowdown of the MOC after oscillations occurs mainly in runs performed with the "world all closed" has not yet been solved.

The feedback mechanism can only occur when the deep water is formed in the GIN Sea. Overall, the location of the region of deep water formation is more important for the oscillations than any other factor. It has been shown that no oscillations occur when the main convection takes place in the subpolar region south of Greenland. This state of the model is more stable during freshwater experiments and does not result in instabilities. However, all three steady states with deep water formation in the GIN Sea had a highly unstable Atlantic

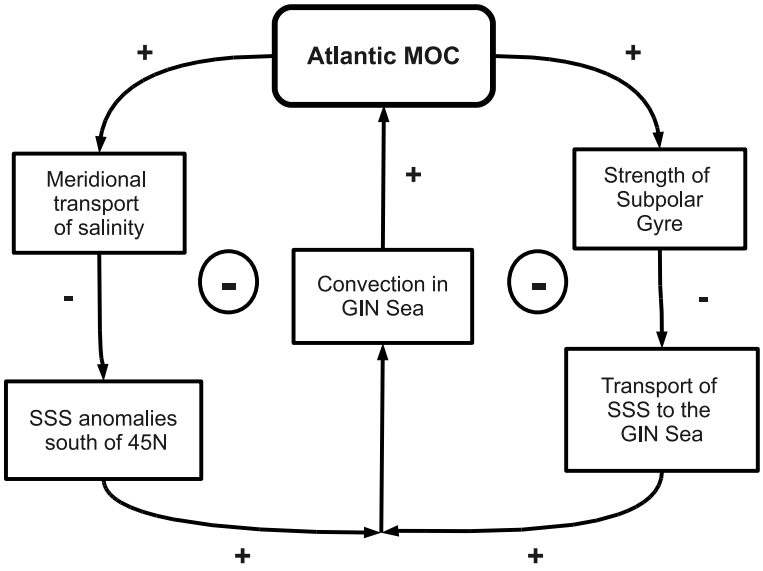

Figure 6.21: Schematic diagram of the physical feedback mechanisms causing the oscillations in the Atlantic MOC. The signs attached to the arrows indicate the correlation between the changes of the quantities in the two boxes. The circled sign indicates the resulting feedback of the whole loop.

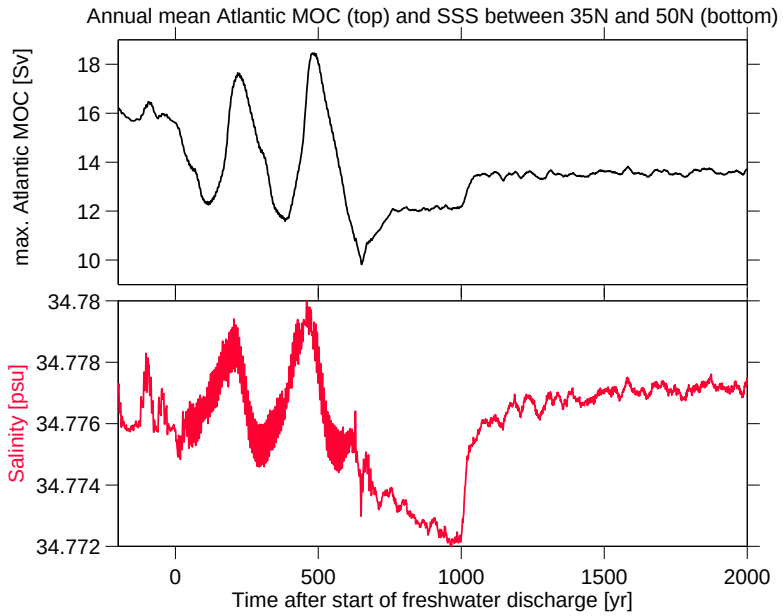

Figure 6.22: Annual mean Atlantic MOC of the run *Oscillation* 2 (top) and the development of SSS in the North Atlantic between 35-50°N during a 1,000 year freshwater perturbation of 0.014 Sv when using the "world all closed" setting. The time series were smoothed with a 10-year running mean.

MOC during perturbation experiments.

6.4 Numerical instability in the model

In the previous section, a feedback mechanism was described which leads to oscillations in the Atlantic MOC. Also the importance of the model steady state and the location of deep water formation was discussed. However, despite the suggested feedback loop, it is also possible that the oscillations may be generated by a numerical instability in the model. This hypothesis would be supported by the finding of the high-frequency SSS variabilities in the Atlantic between 35° and 50°N, which could not be explained by physical means. The aim of this section is to find possible computational problems of the model and to illustrate one way which might prevent oscillations in further model simulations.

6.4.1 The CFL-Criterion

When solving a differential equation in a model, a variety of numerical schemes can be used. They all have certain limitations which have to be accounted for. In explicit discretisation schemes, solutions of previous time steps are used to derive the solution of the new time step. The problems of these schemes are certain limitations on the temporal and spatial resolution of the grid spacing. If the temporal resolution is coarse, as it is the case in the Bern3D model where 48 time steps are calculated per year, the scheme is not able to integrate very fast velocities. This limit is called Courant-Friedrich-Levy (CFL) criterion. It provides the maximum velocity, with which a signal can be transported and the spatial and temporal

resolution of the model. The CFL criterion for a typical advective velocity u is defined as follows:

$$\left|\frac{u\Delta t}{\Delta x}\right| \leq 1, \tag{6.5}$$

where Δt is the length of the time step and Δx indicates the grid along which a tracer is transported with the velocity u. The CFL criterion which needs to be fulfilled for diffusive transport of a given diffusivity K is:

$$\frac{K\Delta t}{(\Delta x)^2} < 0.5. \tag{6.6}$$

If the CFL criterion is not fulfilled for a particular flux in the numerical grid, a numerical instability results from the calculation, which is usually expressed by oscillations in time series. For high transport velocities (large u), an appropriately small time step Δt has to be chosen in order to avoid wrong model results due to instabilities.

The second scheme which is used to calculate differential equations in models is the implicit scheme. In the implicit scheme, no CFL criterion has to be fulfilled, however it is computationally less efficient than the explicit scheme and is therefore only sparsely used in our model.

According to *Müller* [2007], typical advective velocities in the Bern3D ocean model are 0.2 ms^{-1} in the horizontal direction and $3{\times}10^{-5}$ ms^{-1} in the vertical direction. These fluxes are small enough to be calculated by the explicit scheme in our model with the selected Δx and Δt of the model grid. However, due to the diagonal vertical diffusion term, vertical diffusive fluxes do not fulfill the CFL criterion in the Bern3D model and therefore tracer transport in the vertical direction has to be calculated with the implicit scheme.

6.4.2 Changing the time step

According to the limitations given by the CFL criterion, the origin of the oscillations in the MOC could be found in the large time step of the Bern3D model. It is possible that the model has always been running at the upper computational limit. With the opening of the BS and IP, transport velocities have increased marginally, and now the CFL might no longer be fulfilled.

Character	NTS1	NTS2
time steps per year	96	192
amount of freshwater	0.014 Sv	0.014 Sv
duration of perturbation	1,000 years	1,000 years
shape of freshwater pulse	rectangular	rectangular
name of world setting	“world IP closed”	“world IP closed”

Table 6.5: Parameter setup for the runs NTS1 and NTS2 with a time step half and a quarter as large as in the standard model version.

In a first set of two test runs, the time step was temporarily reduced to see whether this has an effect on the occurrence of oscillations in the MOC. The experiments were done with the "world IP closed" since the oscillations in this setup were very pronounced and caused a high variance in the MOC. Tab. 6.5 summarizes the two experiments called NTS1 and NTS2. Note that before the two experiments were performed, a diagnosis of the salt fluxes and a 10,000 year MBC (see section 4.1) had to be recalculated for both new time steps. According to this, the model steady state for these two experiments is a new one. Fig. 6.23 shows the Atlantic MOC after perturbation experiments with a smaller time step. When the time step is set to 96 steps per year (Fig. 6.23a), the MOC still oscillates during the freshwater perturbation. No oscillations can be seen when the time step is a quarter of the original (Fig. 6.23b: 192 steps per year). Here, the MOC reduces the strength by about 1 Sv for the duration of the perturbation and increases again after the end of the freshwater pulse.

The evolution of the MOC, when changing the time step during the freshwater perturbation, is shown in Fig. 6.24. Again, the magnitude of the freshwater forcing was 0.014 Sv, however the duration of the pulse was increased to 3,000 year. Until year 1,000, the model integrated with the original time step of 48. Then the time step was halved at the year 1,000 and quartered

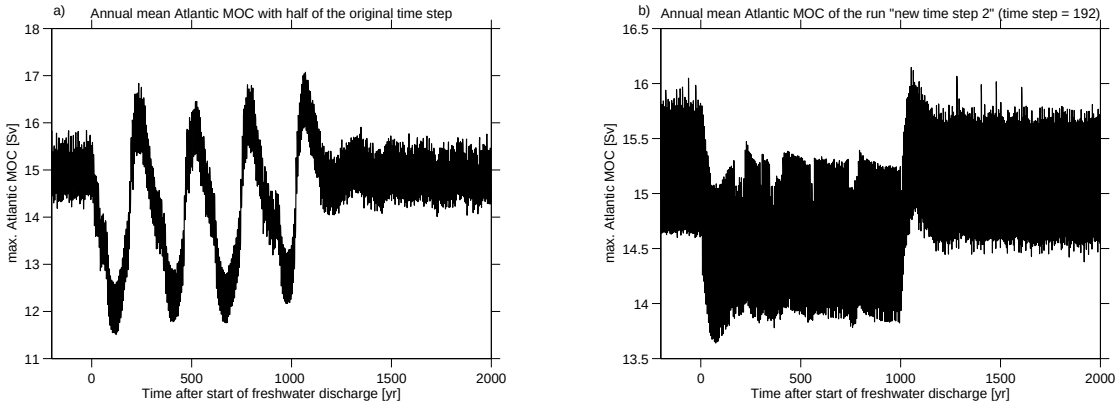

Figure 6.23: Annual mean Atlantic MOC during a 1,000 years freshwater perturbation of 0.014 Sv with a) half of the original time step and b) a quarter of the original time step.

Character	NTS3
amount of freshwater	0.014 Sv
duration of perturbation	3,000 years
freshwater begin	year 0
freshwater end	year 3,000
shape of freshwater pulse	rectangular
time step 48	from yr -500 to yr 1,000
time step 96	from yr 1,000 to yr 2,000
time step 192	from yr 2,000 to yr 4,000
name of world setting	"world IP closed"

Table 6.6: Parameter setup for the run NTS3. A freshwater perturbation of 0.014 Sv was applied during 3,000 years and the time step was reduced during the perturbation.

at the year 2,000. The run is called NTS3 and a detailed overview on the parameter setup of the experiment can be derived from Tab. 6.6. When the time step is reduced to half of the original at the year 1,000 during the perturbation, the amplitude of the oscillation reduces rapidly and after about 500 years, the oscillations vanish more or less. When the time step is reduced once more to only a quarter of the original, no oscillations can be seen anymore. This gives evidence that in fact a smaller time step leads to a more stable MOC where no oscillations can be seen during the perturbation. It is interesting to see that in the time from 2,000 to 3,000 where the time step is smallest, the MOC is slightly stronger, even though the amount of the perturbation stays the same. Also the low-frequency variabilities in the MOC can not be seen anymore when a small time step is used for the model simulations.

In section 6.3.4, the importance of the convection region on the appearance of oscillations was highlighted. Since the two experiments NTS1 and NTS2 have a different steady state to all the others discussed so far, the region of convection needs to be considered. It is possible that no oscillations occur simply because the convection takes place south of Greenland instead of in the GIN Sea, which would make the system more stable. The shuffling convection at the beginning of the experiment for both runs is shown in Fig. 6.25. When dividing the time step, no changes in the region or in the strength of the deep water formation can be seen (Fig. 6.25a). The main sinking of the water into the deep ocean in the North Atlantic takes place in the GIN Sea as it was the case for the other world settings in which oscillations were found. However, when the time step is only a quarter of the original, an additional region of deep convection can be observed in the Labrador Sea (Fig. 6.25b). This finding is very interesting, since in none of the experiments analyzed so far, convection took place in the Labrador Sea. Even though the salinity fields of *Levitus et al.* [1994] were modified to higher values in both the GIN Sea and the Labrador Sea in order to increase deep water formation

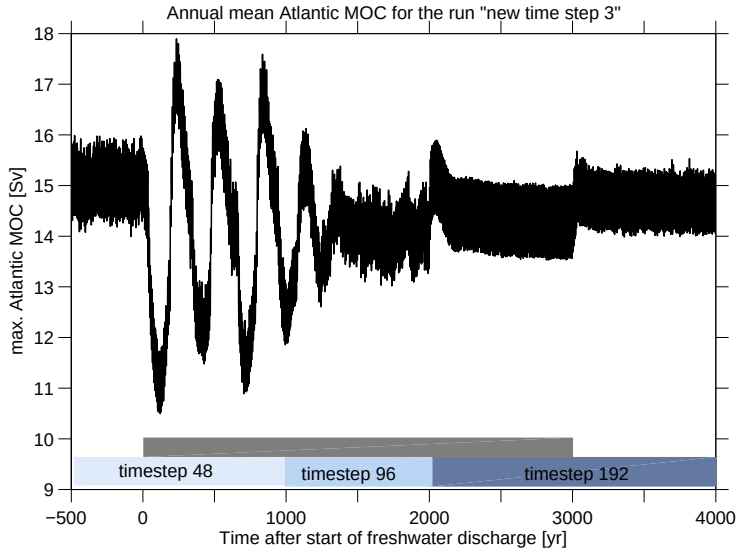

Figure 6.24: Annual mean Atlantic max. MOC with a freshwater perturbation of 0.014 Sv during 3,000 years. Until year 1,000, the model calculation uses the standard time step of 48 integrations per year. The time step is reduced into half the original (96 integrations per year) at year 1,000 and to a quarter (192 integrations per year) at year 2,000. The gray bar indicates the duration of the freshwater perturbation.

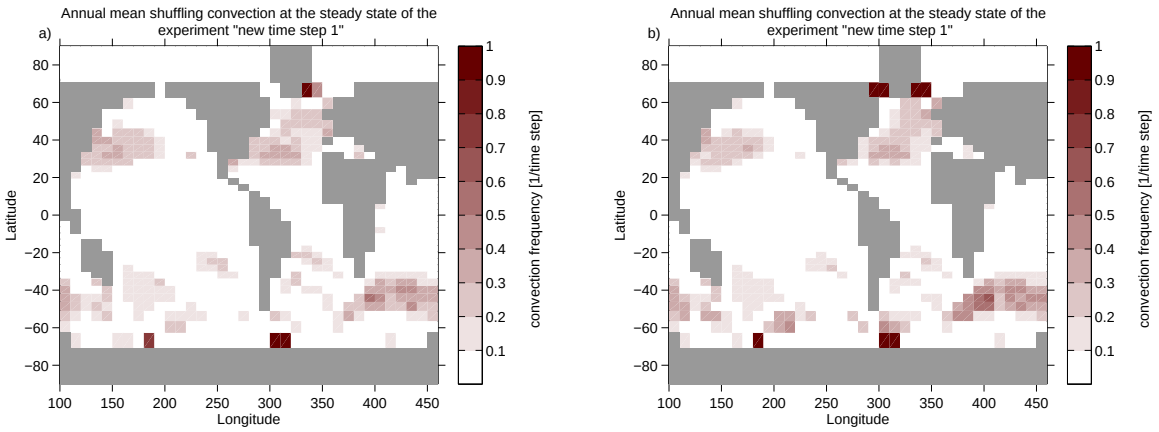

Figure 6.25: Annual mean shuffling convection events per time step in the steady state of the model when computing the model with a) half of the original time step and b) a quarter of the original time step.

there (see section 3.5), the SSS in the Labrador Sea have always been too low in order to produce shuffling convection there. With the small time step, a more realistic steady state is achieved, which is not possible with a time step of only 48 steps per year.

6.4.3 Summary and Conclusion

The importance of choosing a sufficiently small time step in order to fulfill the CFL criterion and to achieve good model results was shown in the previous section. Based on the number of model simulations with smaller time steps, it was found that the overturning circulation is much more stable when the time step is reduced. The sensitivity of the Bern3D model to a smaller time step when using the "new world" is summarized in Fig. 6.26. The time step was either chosen 48 (original), 96 (half of the original) or 192 (quarter of the original) and the amount of freshwater was gradually increased. The runs were classified as described in section 6.2.1, every box represents one experiment. The colors of the colorbar indicate the amplitude of the oscillations when the experiment was classified as *Oscillation Type 1*. Green stands for a complete shutdown of the MOC after the perturbation and gray indicates experiments which were classified as *Weak MOC*. Since oscillations still can be observed when the time step is only half of the original, a reduction to a quarter is needed in order to receive no oscillations in any model simulations.

Also the model steady state is more realistic when the time step is small. In addition to the convection in the GIN Sea, also deep water formation can be observed in the Labrador Sea when when the time step is quartered. The MOC in this new model steady state does not oscillate in any freshwater perturbation experiment. The absence of oscillations can therefore not clearly be assigned to a numerical instability, but can also be due to the new model steady state with additional convection in the Labrador Sea, which stabilizes the Atlantic MOC during freshwater perturbations.

Based on the findings of this section, it is recommended to increase the time step for the Bern3D model to a quarter of the original time step, even though a smaller time step also increases the time which is needed for model simulations by a factor of four. Since one major benefit of our model is the computational efficiency, a reduction of the time step could be

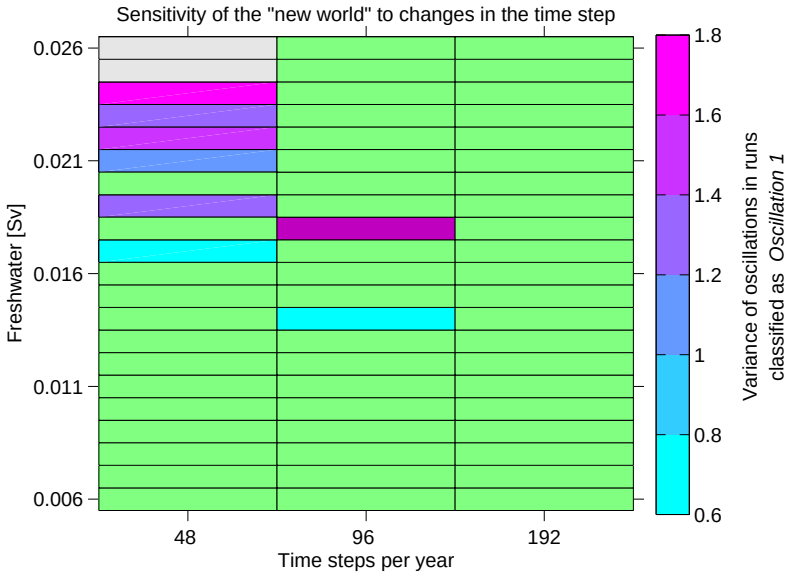

Figure 6.26: Sensitivity of the "new world" to freshwater perturbation and different time steps. The classification of the runs is done according to the description in section 6.2.1. Every color represents a freshwater perturbation experiment with the parameters given in the x-axis (time step) and the y-axis (amount of freshwater [Sv]). The colors in the colorbar represent the variance of the oscillations which appear in the Atlantic MOC. Gray ( ) indicates experiments with no oscillations in the MOC and green ( ) indicates the runs where the Atlantic MOC shuts down right after the start of the perturbation and does not recover anymore.

a major disadvantage. Especially long-term simulations with many tracers would be most negatively affected. A permanent increase of the time step to 192 integrations per year might therefore make not much sense for all simulations. The model spinup or test simulations can still be performed with the original time step. However, it is important to be aware of the limitations of the large time step and to take this into account when analyzing model output of simulations with 48 integrations per year. In order to avoid wrong results, it is recommended to reduce the time step to a quarter of the original when performing simulations which are used for specific analysis or for publications.

Chapter 7

Summary and Outlook

This thesis shows that the Bern3D model, using the "new world" with an open Bering Strait(BS) and Indonesian Passage (IP) and applying a freshwater perturbation in the North Atlantic, has three steady states. Either the Atlantic MOC is in an "on" state, an "intermediate" state or an "off" state. When the freshwater perturbation is above a certain threshold, the MOC can recover on its own from the "off" to the "intermediate" state, otherwise a negative freshwater perturbation is needed in order to switch the circulation to the "on" state. Additionally, oscillations in the Atlantic MOC have been found for small freshwater perturbations.

Three world maps were created to distinguish the effect of the open BS and IP on the occurrence of oscillations. In sensitivity experiments with the different world masks, the effect of changes in the Atlantic-to-Pacific freshwater correction and the wind stress scaling factor on the stability of the Atlantic MOC during freshwater experiments was tested. It has been shown that the two parameters do not lead to an absence of oscillations. However, they cause a shift in the freshwater threshold which is needed to trigger oscillations.

No oscillations were found in the world mask with a closed BS, the Atlantic MOC oscillated when the IP is closed and when both straits are closed. The absence of oscillations in simulations with the "world BS closed" was explained by the location of deep water formation south of Greenland instead of in the GIN Sea, as it is the case for the other three settings. This location of deep water formation is the same as in the "intermediate" state of the MOC. Therefore, it is suggested that deep water formation south of Greenland leads to a more stable Atlantic MOC during freshwater perturbations.

Two possibilities for the origin of the oscillations were analyzed, namely a physical feedback mechanism and a numerical instability in the model. A negative feedback mechanism was suggested to be a possible basis for the occurrence of oscillations. It was shown that a reduced strength in the Atlantic MOC leads to an accumulation of surface salinity in the subtropical Atlantic due to the reduction in meridional transport of surface water. The weak SPG which is linked to the slowdown in the Atlantic MOC increases the transport of the positive SSS anomalies towards the GIN Sea, which results in stronger convection in this region and therefore a resumption of the Atlantic MOC.

It has been shown that by reducing the time step to a quarter of the original 1/48 year, a more stable overturning circulation can be achieved where no oscillations are observed. However, the absence of oscillations in simulations with a small time step could not formally attributed

to a numerical instability in the model, since also the steady state is different when a time step of a quarter of the original is applied. In this new steady state, deep convection also takes place in the Labrador Sea while it was only observed in the GIN Sea when running the model with the standard time step. It seems that the additional region of deep water formation has a stabilizing effect on the Atlantic MOC. It is therefore recommended, to to use a smaller time step for future model simulations, since no oscillations are found and also because deep water formation in the Labrador Sea leads to a more stable Atlantic MOC in the model and overall to a better representation of the water masses.

In order to clearly assign the appearance of oscillations to a numerical problem in the model or to the feedback mechanism which was proposed, the performance of a number of freshwater perturbation experiments with the small time step is needed in order to find the freshwater threshold to cause a shutdown of the Atlantic MOC. The sensitivity of the new model state needs to be tested also with respect to other parameters, e.g., the wind stress scaling factor or the Atlantic to Pacific freshwater correction. Also, the effect of deep water formation in the Labrador Sea on the distribution of tracers in the depth of the ocean needs to be investigated in future experiments. Finally, it would be very interesting to analyze the effect of a reduction in the time step on simulations coupled to the EBM.

List of Tables

List of Figures

Bibliography

Arzel, O., M. H. England, and O. A. Saenko, The impact of wind-stress feedback on the stability of the Atlantic meridional overturning circulation, *Journal of Climate, in press*.

Arzel, O., M. H. England, and W. P. Sijp, Reduced stability of the Atlantic meridional overturning circulation due to wind stress feedback during glacial times, *Journal of Climate, 21*(23), 6260–6282, 2008.

Bacon, S., Circulation and fluxes in the north Atlantic between Greenland and Ireland, *Journal of Physical Oceanography, 27*(7), 1420–1435, 1997.

Barker, S., P. Diz, M. J. Vautravers, J. Pike, G. Knorr, I. R. Hall, and W. S. Broecker, Interhemispheric atlantic seesaw response during the last deglaciation, *Nature, 457*(7233), 1097–1102, 2009.

Biastoch, A., C. W. Boning, and J. R. E. Lutjeharms, Agulhas leakage dynamics affects decadal variability in Atlantic overturning circulation, *Nature, 456*(7221), 489–492, 2008.

Bond, G. C., W. Showers, M. Elliot, M. Evans, R. Lotti, I. Hajdas, G. Bonani, and S. Johnsen, *Mechanisms of Global Climate Change at Millennial Time Scales, Goephys. Monogr. Ser.*, Volume 112, AGU, Washington D. C., 1999.

Böning, C. W., M. Scheinert, J. Dengg, A. Biastoch, and A. Funk, Decadal variability of subpolar gyre transport and its reverberation in the north atlantic overturning, *Geophys. Res. Lett., 33*(21), L21S01–, 2006, September.

Born, A., and A. Levermann, The 8.2 ka event: Abrupt transition of the subpolar gyre toward a modern North Atlantic circulation, *Geochemistry Geophysics Geosysems, 11*, Q06011, 2010.

Broecker, W. S., The biggest chill, *Natural History, 97*, 74–82, 1987.

Broecker, W. S., M. Andree, W. Wolfli, H. Oeschger, G. Bonani, J. Kennett, and P. D., The chronology of the last deglaciation: Implications to the cause of the Younger Dryas event, *Paleoceanography, 3*(1), 1–19, 1988.

De Boer, A. M., and D. Nof, The Bering Strait's grip on the northern hemisphere climate, *Deep Sea Research Part I: Oceanographic Research Papers, 51*(10), 1347–1366, 2004.

Edwards, N., and R. Marsh, Uncertainties due to transport-parameter sensitivity in an efficient 3-D ocean-climate model, *Climate Dynamics, 24*(41), 415–433, 2005.

Edwards, N. R., A. J. Willmott, and P. D. Killworth, On the role of topography and wind stress on the stability of the thermohaline circulation, *Journal of Physical Oceanography, 28*(5), 756–778, 1998.

Ganachaud, A., and C. Wunsch, Improved estimates of global ocean circulation, heat transport and mixing from hydrographic data., *Nature, 408*, 453–457, 2000.

Gerber, M., and F. Joos, Carbon sources and sinks from an Ensemble Kalman Filter ocean data assimilation, *Global Biogeochemical Cycles, 24*, GB3004, 2010.

Gerber, M., F. Joos, M. Vzquez-Rodriguez, F. Touratier, and C. Goyet, Regional air-sea fluxes of anthropogenic carbon inferred with an Ensemble Kalman Filter, *Global Biogeochemical Cycles, 23*, GB1013, 2009.

Häkkinen, S., and P. B. Rhines, Decline of subpolar North Atlantic circulation during the 1990s, *Science, 304*, 555–559, 2004.

Häkkinen, S., and P. B. Rhines, Shifting surface currents in the northern North Atlantic Ocean, *Journal of Geophyical Research, 114*, C04005, 2009.

Hátún, H., A. B. Sandø, H. Drange, B. Hansen, and H. Valdimarsson, Influence of the Atlantic subpolar gyre on the thermohaline circulation, *Science, 309*(5742), 1841–1844, 2005.

Heinrich, H., Origin and consequences of cyclic ice rafting in the northeast Atlantic ocean during the past 130,000 years, *Quaternary Research, 29*(2), 142–152, 1988.

Hemming, S. R., Heinrich events: Massive late Pleistocene detritus layers of the North Atlantic and their global climate imprint, *Reviews of Geophysics, 42*(1), RG1005, 2004.

Kalnay, E., M. Kanamitsu, R. Kistler, W. Collins, D. Deaven, L. Gandin, M. Iredell, S. Saha, G. White, J. Woollen, Y. Zhu, A. Leetmaa, R. Reynolds, M. Chelliah, W. Ebisuzaki, W. Higgins, J. Janowiak, K. C. Mo, C. Ropelewski, J. Wang, R. Jenne, and D. Joseph, The NCEP/NCAR 40-year reanalysis project, *Bulletin of the American Meteorological Society, 77*(3), 437–471, 1996.

Knutti, R., and T. F. Stocker, Limited predictability of the future thermohaline circulation close to an instability threshold, *Journal of Climate, 15*(2), 179–186, 2002.

Levermann, A., and A. Born, Bistability of the Atlantic subpolar gyre in a coarse-resolution climate model, *Geophyical Research Letters, 34*, L24605, 2007.

Levitus, S., and T. Boyer, NOAA Atlas NESDIS 4: World ocean atlas 1994, *U.S. Departement of Commerce: National Oceanic and Atmospheric Administration, Tech. Rep., Volume 4: Temperature*, 1994.

Levitus, S., R. Burgett, and T. Boyer, NOAA Atlas NESDIS 3: World ocean atlas 1994, *U.S. Departement of Commerce: National Oceanic and Atmospheric Administration, Tech. Rep., Volume 3: Salinity*, 1994.

McManus, J. F., R. Francois, J.-M. Gherardi, L. D. Keigwin, and S. Brown-Leger, Collapse and rapid resumption of Atlantic meridional circulation linked to deglacial climate changes, *Nature, 428*(6985), 834–837, 2004.

Müller, S. A., 2007, *Large-Scale Ocean Circulation, Air-Sea Gas Exchange, and Carbon Isotopes in a Three-Dimensional, Computationally Efficient Ocean Model*, Ph. D. thesis, University of Bern, Institute for Climate and Environmental Physics.

Müller, S. A., F. Joos, N. R. Edwards, and T. F. Stocker, Water mass distribution and ventilation time scales in a cost-efficient, three-dimensional ocean model, *Journal of Climate, 19*(21), 5479–5499, 2006.

Müller, S. A., F. Joos, N. R. Edwards, and T. F. Stocker, Modeled natural and excess radiocarbon: Sensitivities to the gas exchange formulation and ocean transport strength, *Global Biogeochemical Cycles, 22*, GB3011, 2008.

Muscheler, R., F. Joos, J. Beer, S. A. Müller, M. Vonmoos, and I. Snowball, Reply to the comment by Bard et al. on 'Solar activity during the last 1000 yr inferred from radionuclide records', *Quaternary Science Reviews, 26*(17-18), 2304–2308, 2007.

NGRIP, High-resolution record of Northern Hemisphere climate extending into the last interglacial period, *Nature, 431*, 147–151, 2004.

NOAA, National Geophysic Data Center, B. C., 1988, Data announcement 88-mgg-02, digital relief of the surface of the earth.

Nof, D., Does the wind control the import and export of the South Atlantic?, *Journal of Physical Oceanography, 30*(11), 2650–2667, 2000.

Parekh, P., F. Joos, and S. A. Mller, A modeling assessment of the interplay between aeolian iron fluxes and iron-binding ligands in controlling carbon dioxide fluctuations during Antarctic warm events, *Paleoceanography, 23*, PA4202, 2008.

Pond, S., and G. L. Pickard, *Introductory Dynamical Oceanography* (2nd edition ed.)., Butterworth-Heinemann, 1983.

Press, W. H., S. A. Teukolsky, W. T. Vetterling, and B. P. Flannery, *Nummerical Recipes in Fortran 90: The Art of Scientific Computing*, Cambridge University Press, 1992.

Rahmstorf, S., Ocean circulation and climate during the past 120,000 years, *Nature, 419*(6903), 207–214, 2002.

Rahmstorf, S., M. Crucifix, A. Ganopolski, H. Goosse, I. Kamenkovich, R. Knutti, G. Lohmann, R. Marsh, L. A. Mysak, Z. Wang, and A. J. Weaver, Thermohaline circulation hysteresis: A model intercomparison, *Geophys. Res. Lett., 32*(23), 2005, December.

Read, J. F., CONVEX-91: Water masses and circulation of the northeast Atlantic subpolar gyre, *Progress in Oceanography, 48*(4), 461–510, 2000.

Richter, I., and S.-P. Xie, Moisture transport from the Atlantic to the Pacific basin and its response to North Atlantic cooling and global warming, *Climate Dynamics, 35*(2), 551–566, 2010.

Ritz, S. P., 2007, Global distribution of radiocarbon during changes of the Atlantic meridional overtruning circulation, Master's thesis, Universität Bern, Climate and Environmental Physics.

Ritz, S. P., T. F. Stocker, and F. Joos, A coupled dynamical ocean - energy balance atmosohere model for paleoclimate studies, *Journal of Climate, 24*, 349–375, 2011.

Ritz, S. P., T. F. Stocker, and S. A. Müller, Modeling the effect of abrupt ocean circulation change on marine reservoir age, *Earth and Planetary Science Letters, 268*(1-2), 202–211, 2008.

Schulz, M., M. Prange, and A. Klocker, Low-frequency oscillations of the Atlantic Ocean meridional overturning circulation in a coupled climate model, *Climate of the Past Discussions, 2*(5), 801–830, 2006.

Siddall, M., T. F. Stocker, G. M. Henderson, F. Joos, M. Frank, N. R. Edwards, S. P. Ritz, and S. A. Müller, Modeling the relationship between ^{2}31Pa/^{2}30Th distribution in North Atlantic sediment and Atlantic meridional overturning circulation, *Paleoceanography, 22*, PA2214, 2007.

Stocker, T. F., Past and future reorganizations in the climate system, *Quaternary Science Reviews, 19*(1-5), 301–319, 2000.

Stocker, T. F., and S. J. Johnsen, A minimum model for the bipolar seesaw, *Paleoceanography, 18*, 1087, 2003.

Stocker, T. F., and O. Marchal, Abrupt climate change in the computer: Is it real?, *PNAS, 97*(4), 1362–1365, 2000.

Stocker, T. F., and D. G. Wright, Rapid transitions of the ocean's deep circulation induced by changes in surface water fluxes, *Nature, 351*(6329), 729–732, 1991.

Stommel, H., The abyssal circulation, *Deep Sea Research, 5*, 80–82, 1958.

Talley, L. D., Freshwater transport estimates and the global overturning circulation: Shallow, deep and throughflow components, *Progress In Oceanography, 78*(4), 257–303, 2008.

Tschumi, T., F. Joos, and P. Parekh, How important are Southern Hemisphere wind changes for low glacial carbon dioxide? A model study, *Paleoceanography, 23*, PA4208, 2008.

Weijer, W., W. P. M. De Ruijter, and H. A. Dijkstra, Stability of the Atlantic overturning circulation: Competition between Bering Strait freshwater flux and Agulhas heat and salt sources, *Journal of Physical Oceanography, 31*(8), 2385–2402, 2001.

Winton, M., and E. S. Sarachik, Thermohaline oscillations induced by strong steady salinity forcing of ocean general-circulation models, *Journal of Physical Oceanogaphy, 23*, 1389–1410, 1993.

Yoshimori, M., C. Raible, T. F. Stocker, and M. Renold, Simulated decadal oscillations of the Atlantic meridional overturning circulation in a cold climate state, *Climate Dynamics, 34*(1), 101–121, 2010.

Zaucker, F., and W. S. Broecker, The influence of atmospheric moisture transport on the fresh water balance of the Atlantic drainage basin: General circulation model simulations and observations, *Journal of Geophyical Research, 97*, 2765–2773, 1992.

Zaucker, F., T. F. Stocker, and W. S. Broecker, Atmospheric freshwater fluxes and their effect on the global thermohaline circulation, *Journal of Geophyical Research, 99*, 12443–12457, 1994.

Acknowledgments

I would like to thank ...

... Thomas Stocker for giving me the opportunity to write my thesis at the Climate and Environmental Physics department, for all the stimulating inputs and the support during the process of writing the thesis.

... Christoph Raible for introducing me to Linux, for always having an open ear and for his patience in explaining technical details.

... Stefan Ritz for introducing me to Matlab, Fortran and the Bern3D model. He always had the time and the patience to discuss problems and to give useful inputs. I would also like to thank for proof-reading my thesis.

... Raphael Roth for assisting with figures, for proof-reading and for encouraging me in difficult times.

... my family and my friends for their support and patience during my studies.